Static Analysis of Masonry Arched and Buttressed Retaining Walls

Defne Dogu

SAHC

ADVANCED MASTERS IN STRUCTURAL ANALYSIS
OF MONUMENTS AND HISTORICAL CONSTRUCTIONS

Master's Thesis

Defne Dogu

**Static Analysis of Masonry
Arched and Buttressed
Retaining Walls**

UPC
UNIVERSITAT POLITÈCNICA
DE CATALUNYA

University of Minho

Spain | 2019

ARCCHIP

ADVANCED MASTERS IN STRUCTURAL ANALYSIS
OF MONUMENTS AND HISTORICAL CONSTRUCTIONS

Master's Thesis

Defne Dogu

Static Analysis of Masonry Arched and Buttressed Retaining Walls

DECLARATION

Name: Defne Dogu

Email: defnedogu193@gmail.com

Title of the
Msc Dissertation: Static Analysis of Masonry Arched and Buttressed Retaining Walls

Supervisor(s):   Climent Molins and Nirvan Makoond

Year: 2019

I hereby declare that all information in this document has been obtained and presented in accordance with academic rules and ethical conduct. I also declare that, as required by these rules and conduct, I have fully cited and referenced all material and results that are not original to this work.

I hereby declare that the MSc Consortium responsible for the Advanced Masters in Structural Analysis of Monuments and Historical Constructions is allowed to store and make available electronically the present MSc Dissertation.

University: Technical University of Catalonia

Date: 16.07.2019

Signature:

This page is left blank on purpose.

ACKNOWLEDGEMENTS

This page is left blank on purpose.

ABSTRACT

Retaining walls are presumably the oldest engineering solutions of laterally supporting soil masses at locations of elevation change. Mur Casa Salvans is a masonry retaining wall with arches and buttresses, which was built in 1909 and located in Terrassa, Spain. The wall contains a series of 11 arches of unique shapes, dimensions and inclinations connected by buttresses.

The stability of the wall was evaluated from the perspective of modern retaining wall design principles. As the stability of a retaining wall is contingent upon the geometry of the wall, accurate geometrical representation is of vital importance. Three-dimensional models of the front of the wall, obtained through photogrammetry, were combined with available information from previously performed laser scanning and topographic survey to construct the cross sections of the wall. Due to the complex geometry of the structure, the analysis was carried out on unit sections between the vertical axis of the buttress and the key of the adjacent arch.

A practical tool was developed to assess the stability of the retaining walls of the given typology in terms of overturning, sliding and base pressures. As a consequence of the uncertainties related to the soil parameters and the buried elements of the wall, the factors did not comply with modern design criterion. A sensitivity analysis was carried out on the shear strength parameters of the backfill namely, the soil friction angle, φ and the friction angle of the wall and the soil δ. It was found out that slight increases in both values enhance the factors defining stability significantly and decrease the base pressures.

The safety of the arches was verified according to the Lower Bound Theorem by applying graphic statics on the arch series. Thrust lines were located within the boundaries of each arch by considering their actions against each other.

This page is left blank on purpose.

RESUM

Els murs de conteniment de terres de fàbrica és probablement la solució d'enginyeria més antiga per donar suportar lateral a les masses de sòl en els canvis d'elevació. El mur de la Casa Salvans és un mur de contenció de maçoneria amb arcs i contraforts, construït el 1909 i situat a Terrassa, Catalunya. La paret conté una sèrie d'onze arcs de formes, dimensions i inclinacions diferents connectades per contraforts.

L'estabilitat de la paret s'avalua des de la perspectiva dels principis moderns de disseny dels murs de contenció. Com l'estabilitat d'un mur de contenció depèn de la geometria de la paret, la representació geomètrica precisa és de vital importància. Els models tridimensionals de la part frontal de la paret, obtinguts mitjançant fotogrametria, es van combinar amb la informació disponible de l'exploració làser i l'aixecament topogràfic existent per construir les seccions transversals de la paret. A causa de la complexa geometria de l'estructura, l'anàlisi es realitza en seccions individualitzades entre l'eix vertical del contrafort i la clau de l'arc adjacent.

S'ha desenvolupat una eina pràctica per avaluar l'estabilitat dels murs de contenció de la tipologia en qüestió en termes de bolcada, lliscament i pressions de base. Com a conseqüència de les incerteses relacionades amb els paràmetres del sòl i els elements enterrats de la paret, els factors de seguretat no compleixen els criteris moderns de disseny. S'han desenvolupat anàlisis de sensibilitat sobre els paràmetres de resistència al tall del terreny, és a dir, l'angle de fricció del sòl, φ i l'angle de fricció de la paret i el sòl δ. S'ha comprovat que petits increments en ambdós valors milloren significativament els factors que defineixen l'estabilitat i disminueixen les pressions de la base.

La seguretat dels arcs s'ha verificat segons el teorema del límit inferior aplicant l'estàtica gràfica a la sèrie d'arcs. Les línies d'empenta es troben dins dels límits de cada arc tenint en compte l'empenta a través de tot el sistema d'arcs.

This page is left blank on purpose.

ADVANCED MASTERS IN STRUCTURAL ANALYSIS OF MONUMENTS AND HISTORICAL CONSTRUCTIONS

TABLE OF CONTENTS

List of Figures

List of Tables

List of Symbols

σ Normal Stress

σ' Effective Stress

K_0 At-rest Earth Pressure Coefficient

γ Specific Weight

P_0 Resultant Force of Earth Pressure

q Surcharge Pressure

φ Soil Friction Angle

δ Soil - Backfill Friction Angle

c Cohesion

c_u Undrained Cohesion

c_w Wall Adhesion

P_a Total Active Thrust

K_a Active Earth Pressure Coefficient

α Angle of the back of the wall

β Backfill Slope

P_p Total Passive Resistance

K_p Passive Earth Pressure Coefficient

R_v Resultant Vertical Force

q_{ult} Soil Bearing Capacity

1   INTRODUCTION

Retaining walls are used to hold soil in place at locations of abrupt elevation change since the ancient times. The tremendous capacity of gravity retaining walls in resisting earth pressures, hydrostatic pressure, surcharge loads and other external loads relies mainly on their geometry and weight. The difference of Mur Casa Salvans from a conventional gravity retaining wall is due to the engagement of the arches and the buttresses. It is a spectacular example of a common typology of retaining walls that restrain hard, unsaturated soils by the use of series of arches connected at buttresses. The arches have an instrumental role in load transmission to the buttresses, which are significantly thicker than the wall, enabling the use of less material throughout the wall. By virtue of the buttresses in the longitudinal direction, the wall can have a greater height. This allows such walls to be more slender and have a smaller cross section compared to other gravity retaining wall coequals.

This thesis aims to develop a methodology to assess the stability of the retaining walls of the given typology using modern retaining wall design principles, based on the application on Mur Casa Salvans. Mur Casa Salvans, located in Terrassa, Spain, is a masonry retaining wall made of pebble stones bonded by mortar, dating back to 1909. The wall has a total length of 144 m and a maximum height of 11.5 m. The thesis focuses on the section of the wall having a series of 11 arches that each has a unique shape, dimensions and inclination (Figure 1).

| (a) | (b) |

Figure 1. (a) Large arches of Mur Casa Salvans (b) Small arches of Mur Casa Salvans

Due to the reliance of the stability of a retaining wall on the geometry itself, accurate identification of the complex geometry is essential in this study. Three-dimensional information about the front of the wall, especially the inclinations which could not be determined accurately by other methods, will be gathered for each individual arch by means of photogrammetry. Photogrammetry is a powerful, non-contact measuring tool that can be used to obtain accurate physical information of any kind of object.

Furthermore, it is one of the most cost-effective and portable approaches as the data is collected by using a consumer level digital camera.

In the sequel, three-dimensional models of the front of the wall will be created in sections. Previously available laser scanning data and measurements taken on site will be used to ensure the accuracy of the models to be used for stability analysis.

In accordance with the load transmission from the arches to the buttresses, hypothetical cross sections, of representative units, to be analyzed for stability will be constructed by combining the 3-D models with the available information from a topographic survey. Due to the redundancy of the uncertainties related to the characteristics of the buried elements and excessive variations in geometry, conservative assumptions will be made when required.

A practical tool to assess the stability of the wall in terms of overturning, sliding and base pressures will be developed, and the analyses will be carried out on the unit sections of the wall. The tool aims to analyze the stability of any retaining wall of the particular typology, if required inputs related to geometry, material and soil characteristics are available.

As earlier retaining walls were not designed to comply with modern design criterion and a consequence of the conservative assumptions made on the geometry together with the uncertainties related to soil parameters, the results will not be interpreted as safety indicators. Since the shear strength parameters of the soil were derived indirectly through correlations with other tests, it is interesting to determine the sensitivity of the stability factors on those, by performing a parametric analysis.

Finally, the stability of the arches will be assessed by applying two-dimensional graphic statics on the arch series to verify the safety of the series by determining a possible scenario of interconnected thrust lines. By this manner, the knowledge on the working principle of the wall will be enhanced by determining the load path between the arches.

2 STATE OF ART

2.1 Retaining Walls

Retaining walls are structures that laterally support slopes of soil, rock or other materials which would collapse in a natural configuration, in the absence of a retaining structure. They are frequently used to prevent landslides and erosion, mitigate the existing phenomena, support bridge approaches, protect structures and to provide large flat surfaces for construction.

They can be classified into two broad categories such as gravity or freestanding walls and embedded walls. The stability of a gravity wall is due to the self-weight of the wall itself whereas for an embedded wall, it is based on the passive resistance of the soil over embedment depth or external supports. Figure 2 illustrates two examples from both categories.

(a)   (b)
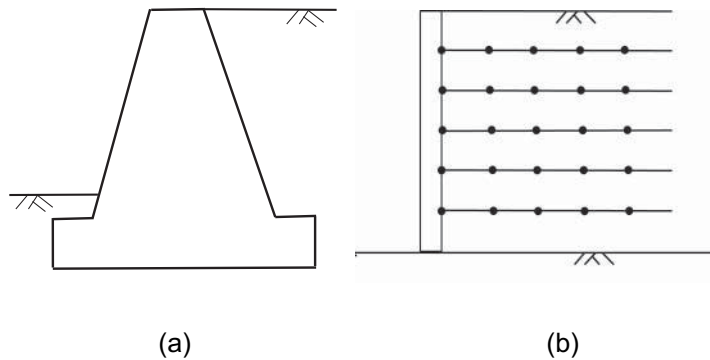
Figure 2. (a) Traditional gravity retaining wall. (b) Mechanically stabilized earth wall [1]

Traditional gravity walls are massive walls of masonry or concrete which are quite uneconomical due to excessive material requirement for sufficient dead load. Furthermore, the height is quite limited as increasing the height brings up additional soil mass to be retained.

A more feasible type of freestanding walls, which are frequently used nowadays, are cantilever retaining walls. Introducing a cantilever arm at the base of the wall, benefits from the weight of the backfill above the arm while maintaining stability (Figure 3). Due to the contribution of the backfill, they require less material compared to gravity retaining walls. Furthermore, the cantilever arm also enhances the sliding resistance of the wall due to increased surface area of the base. Additional stabilizing forces enable cantilever walls to be taller than the traditional ones. Even though they usually have inverted "T" or "L" shapes, more complex geometry is also possible by introducing counterforts or buttresses. Counterforts are struts connecting the wall to the cantilever arm at the heel while buttresses are located at the front side of the wall with the same purpose (Figure 4). Introducing these structural components further reduces the material requirement, allowing the wall in between the struts to be thinner and taller. Other types of gravity retaining walls include gabion and crib walls both

of which are composites of different materials. Gabion walls are usually in the form of steel mesh cages filled with cobble sized particles while crib walls are open structures constructed by assembling precast concrete or timber members with coarse-grained filling material. [1][2][3][4]
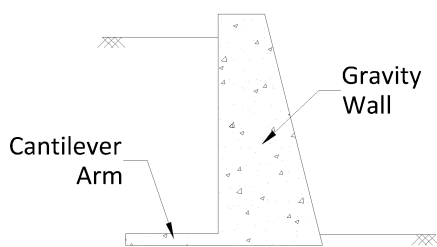
Figure 3. Difference between cantilever and gravity walls [2]
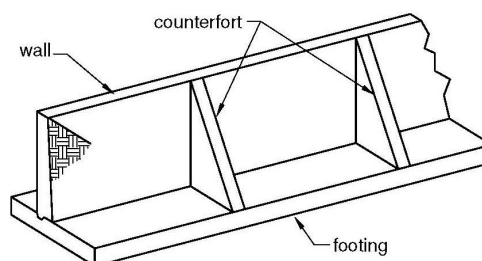
Figure 4. Cantilever wall with counterforts [3]

2.2   Lateral Earth Pressures

A retaining wall is aimed to resist the lateral earth pressure exerted by the soil mass behind the structure. The lateral earth pressures are classified based on the movement direction of the retaining structure relative to the soil, such as:

1. *At-rest earth pressure*, when there is no relative movement between the retaining wall and the soil mass. Thus, the lateral strain in the soil is zero.
2. *Active earth pressure,* when the retaining wall moves away from the soil mass, resulting in a decrease in horizontal stress in the soil as it expands outwards.
3. *Passive earth pressure,* when the retaining wall moves towards the soil mass, followed by an increase in horizontal stress due to lateral compression of the soil.

At-rest earth pressure is expressed in terms of effective stress as follows

$$\sigma_0 = K_0 \sigma'$$
(1)

where σ_0 is the earth pressure at-rest, K_0 is the coefficient of at-rest earth pressure and σ' is the effective vertical stress in the backfill, along the wall.

The effective vertical stress is calculated as follows

$$\sigma' = \gamma' z = (\gamma_{sat} - \gamma_w). H$$
(2)

where γ' is the buoyant unit weight and γ_{sat} is the saturated unit weight of the soil, γ_w is the unit weight of the water and H is the depth.

Therefore, when the type of backfill is the same throughout the wall, at-rest earth pressure varies linearly with depth as shown in Figure 5. The total resultant force per unit length of the wall due to earth pressure, P_0 equals to the area of the pressure distribution diagram, applied at H/3 above the base of the wall.

$$P_0 = \frac{1}{2} K_0 \gamma' H^2$$

(3)
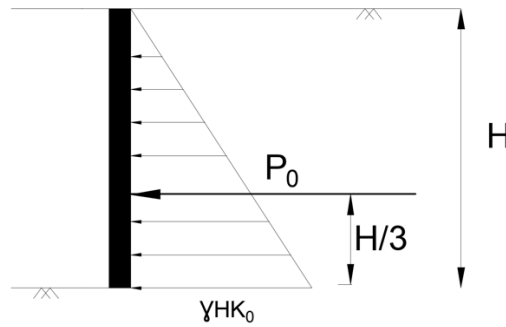
Figure 5. At-Rest Pressure Distribution Diagram

The active and passive earth pressures are also expressed in terms of effective stress as shown in Equation (1) but with their respective pressure coefficients such as the active earth pressure coefficient, K_a for active pressure and the passive earth pressure coefficient, K_p for the passive pressure. Both pressures are distributed along their height of application similarly to the at-rest earth pressure. The force per unit length of the wall due to active pressure is called total active thrust, P_a while the latter is referred to as the total passive resistance, P_p.

Due to being associated with the lateral expansion of the soil, active earth pressure is a minimum value whereas passive earth pressure is a maximum value due to the opposite nature of the action, both of which are referred as limit pressures. The lateral earth pressures are determined based on the Limit Equilibrium Principle. For both cases, a failure shear surface is considered to be developed in the backfill and the failure occurs when there is sufficient movement of the wall. The lateral strain required to activate the passive pressure is significantly larger than the requirement to activate the active pressure (Figure 6).
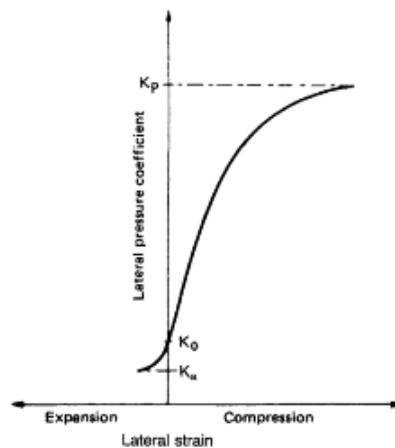
Figure 6.Lateral pressure coefficient lateral strain relation [4]

When there is a uniformly distributed surcharge pressure of q/m^2 applied over the soil surface, the vertical stress, σ increases by q at any depth. Therefore, additional pressure of K_aq should be considered in the active case and K_pq should be considered in the passive case, both of which have constant distributions over the depth. These pressures on a vertical wall surface of height H have resultant forces of K_aqH and K_pqH respectively, applied at H/2 (Figure 7). [1][3][4]
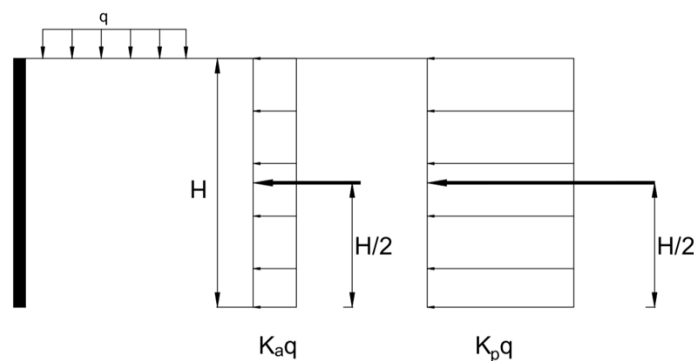
Figure 7.Pressure distribution diagram due to surcharge, q

2.3   Theory of Earth Pressure

There are two common theories that are used to compute earth pressures, Rankine's and Coulomb's Theories of Earth Pressure. Rankine's approach can be interpreted as a simplified version of Coulomb's as it assumes a vertical and smooth back face of the wall and no friction at wall-soil interface.

Coulomb's theory aims to determine the active and passive earth forces acting on a retaining wall by considering the force equilibrium on a soil wedge between the wall and a trial failure surface when it is in a limit equilibrium state. The theory considers important parameters like the inclination of the backfill, inclination of the back of the wall, friction between the backfill and the wall. It adopts the

assumptions of a planar failure surface, isotropic, homogeneous and cohesionless soil and a rigid failure wedge that undergoes translation. Since the theory is based on force equilibrium, it does not provide the earth pressure distributions, but the resultant forces associated with them. Figure 8 illustrates the forces considered to be in equilibrium, for the active and passive cases.

(a)   (b)
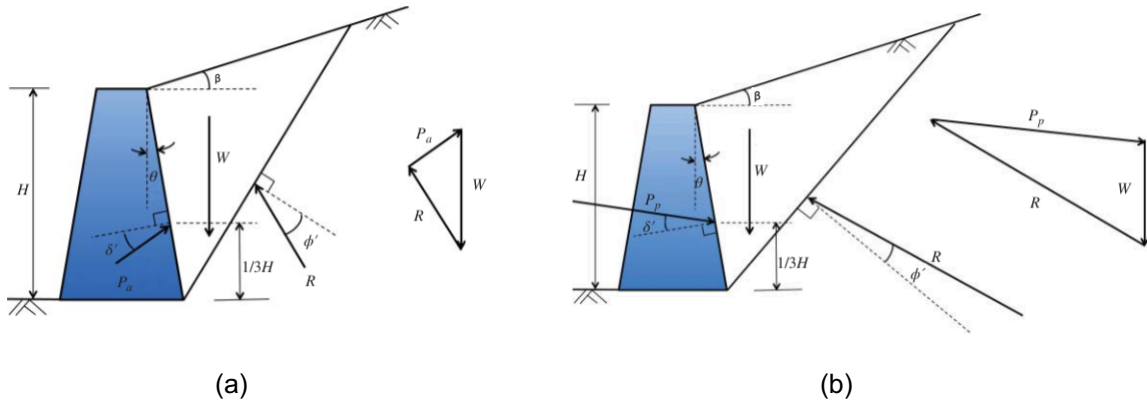
Figure 8. Coulomb's Theory for (a) active case (b) for passive case [1]

The angle of friction between the wall and the backfill material, denoted by δ can be determined by Direct Shear Test performed in laboratory. In the absence of laboratory testing, δ can be correlated to values ranging between 1/2 to 2/3 of the soil friction angle, φ. The wall adhesion, c_w is the second parameter that contributes to shearing resistance.

The theory may be applied to cohesive soils by considering the failure plane extending to the bottom of the tension crack zone (Figure 9) [4]. In that case, another shear strength parameter, cohesion also provides additional resistance against failure.
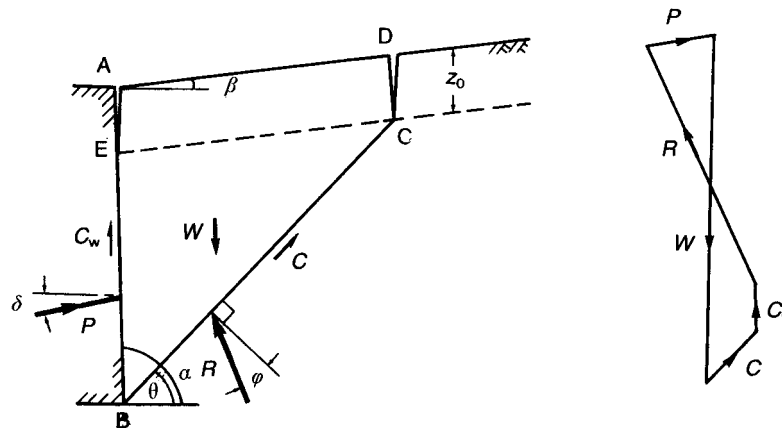
Figure 9.Coulomb's Earth Pressure Theory for active case for cohesive soils [4]

The actual failure surfaces are curved close to the bottom of the wall due to wall friction, both in the active and passive cases (Figure 10). The planar failure surface assumption yields a small error for the active case since its curvature is relatively small in reality and also for the passive case when δ is less

than φ/3. However, especially for high δ and φ values, the theory is not applicable for the passive case due to the increased error. In other words, the theory underestimates the total active thrust and overestimates the total passive resistance.

(a)   (b)
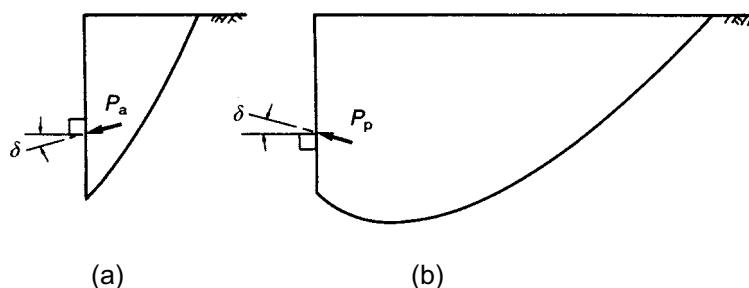
Figure 10. Actual failure surfaces for (a) active and (b) passive cases [4]

In the active case, the soil wedge has a tendency to slide down the failure plane at failure. Thus, the reaction force between soil and the wall acts at an angle δ below the normal to the wall (Figure 10). At failure, when the shear strength of the soil is in full contribution, the reaction on the failure plane acts at an angle φ below the normal to the plane (Figure 8).

Since the directions of all the forces acting on the wedge and the magnitude of W, c_w and c are known, P for the trial failure plane is determined from the force diagram. By repeating the procedure for several failure planes, the maximum P is identified as the total active thrust on the wall. As mentioned earlier in Section 2.2 the total active thrust P_a can be calculated using Equation (3) as follows

$$P_a = \frac{1}{2} \cdot \gamma \cdot H^2 \cdot K_a \tag{4}$$

Coulomb derives the equation for active pressure coefficient as follows. By the use of the sine rule, P can be expressed in terms of the known variables, the weight and the angles of the force diagram. Then, the maximum value of P for a specific α, the angle of the back of the wall, is calculated by $\partial P / \partial \alpha = 0$, yielding the equation of K_a as

$$K_a = \frac{\sin^2(\alpha + \phi)}{\sin^2 \alpha \sin(\alpha - \delta) \left[1 + \sqrt{\frac{\sin(\phi + \delta) \sin(\phi - \beta)}{\sin(\alpha - \delta) \sin(\alpha + \beta)}} \right]^2} \tag{5}$$

where α is the angle of the back of the wall, φ is the soil friction angle, δ is the friction angle between soil and the wall and β is the slope of the backfill.

Conversely, in the passive case, the soil wedge tends to move upwards along the failure plane. Therefore, in order to resist this movement, the reaction P and R act at angles of δ and φ above the normal to the wall surface and to the failure plane, respectively (Figure 8). Following the same procedure described for active case, the total passive resistance is calculated as follows

$$P_p = \frac{1}{2} \cdot \gamma \cdot H^2 \cdot K_p \tag{6}$$

where

$$K_p = \frac{\sin^2(\alpha - \phi)}{\sin^2 \alpha \sin(\alpha + \delta)\left[1 - \sqrt{\dfrac{\sin(\phi + \delta)\sin(\phi + \beta)}{\sin(\alpha + \delta)\sin(\alpha + \beta)}}\right]^2} \tag{7}$$

2.4 Retaining Wall Design Principles

The retaining walls are designed based on the possible failure modes of the corresponding structures namely by overturning, sliding and bearing (Figure 11). For each failure mode, there are safety factors defined to ensure the stability of the structure. A factor of safety is the ratio of the sum of the forces or moments resisting against failure to the corresponding ones causing failure. Commonly, the lateral earth pressure due to the retained soil, surcharge loads and hydrostatic pressure are the failure agents while the self-weight, the friction at the wall-soil interface and the passive resistance at the toe of the wall are the stabilizing ones.

A factor of safety of 1.0 indicates that the structure is in an equilibrium state where any disturbance might lead to failure. Therefore, soil retaining structures are designed for factors of safety greater than one specified by the standards.

Overturning Failure

Sliding Failure

Bearing Capacity Failure

(a)   (b)   (c)
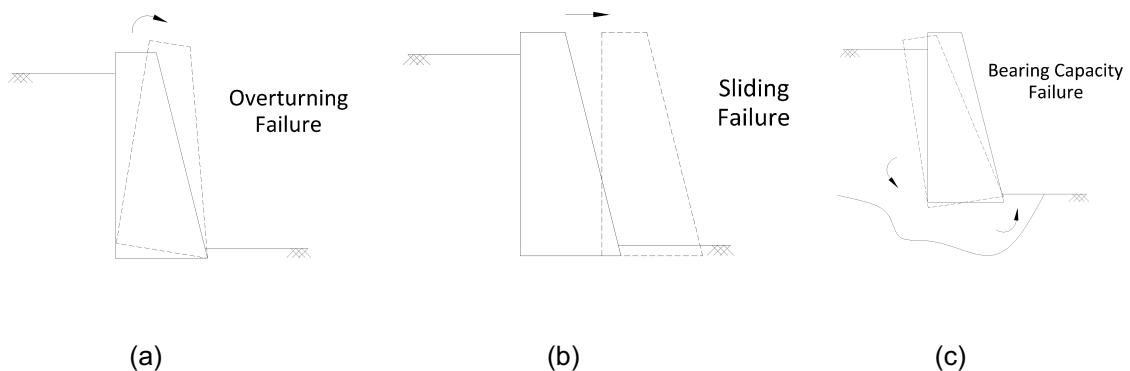
Figure 11. Failure modes of a retaining wall: (a) overturning (b) sliding (c) bearing capacity [2]

The design procedure is initiated by determining all the forces acting on the structure that are constituents of the resultant acting on the base of the wall. Considering a minimum surcharge pressure of 10 kN/m^2 acting on the soil surface behind the wall is recommended. [4]

The point of application of the resultant force at the base is determined by dividing the net moment about any point on the base by the vertical component of the resultant.

$$x = \frac{\Sigma M_{Resisting} - \Sigma M_{Overturning}}{R_v} \qquad (8)$$

where $\Sigma M_{Resisting}$ is the sum of resisting moments, $\Sigma M_{Overturning}$ is the sum of overturning moments and R_v is the vertical component of the resultant force.

If the resultant is within the middle third of the base width, the eccentricity, e does not exceed 1/6 of the base width, the base pressure remains compressive over the entire base. This criterion ensures that the wall is not overturning. If not, negative pressure, thus tension will develop at the base resulting in separation of the footing and the underlaying soil. In other words, only the partial area of the footing is contributing to resistance, which is not desired (Figure 12).
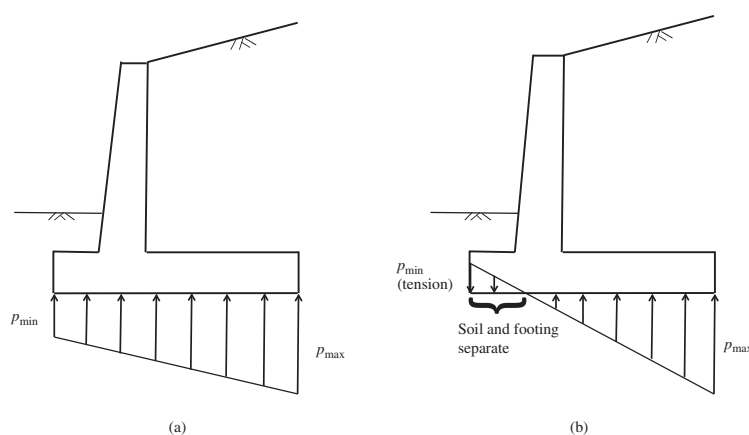
Figure 12. Base pressure distributions for (a) e ≤ B/6 and (b) e> B/6 [1]

The maximum and minimum base pressures when the resultant is within the middle third of the base are calculated as shown in Equation (9).

$$\sigma_{max,min} = \frac{R_v}{B.L}\left(1 \pm \frac{6e}{B}\right) \qquad (9)$$

where $\sigma_{max,min}$ are the maximum and minimum base pressures, R_v is the vertical component of the resultant force, e is the eccentricity, B is the base width and L is the base length.

Although it is not desirable, the maximum base pressure when the resultant is outside the middle third is calculated as shown in Equation (10).

$$\sigma_{max} = \frac{4R_v}{3.L(B - 2e)} \qquad (10)$$

The factor of safety against bearing capacity is determined as the ratio of the maximum base pressure to the bearing capacity of the soil beneath.

$$FS_{bearing} = \frac{q_{ult}}{\sigma_{max}} \tag{11}$$

where q_{ult} is the ultimate bearing capacity of the foundation soil.

The retaining wall is expected to rotate around the toe of the footing. Therefore, the factor of safety against overturning is determined by dividing the sum of the stabilizing moments to the sum of the overturning moments about that point.

$$FS_{overturning} = \frac{\Sigma M_{Stabilizing}}{\Sigma M_{Overturning}} \tag{12}$$

Finally, the factor of safety against sliding is determined as the ratio of the sum of the sliding forces to the sum of the resisting ones as shown in Equation (13). In order to be conservative, the passive pressure at the front of the toe can be neglected.

$$F_{sliding} = \frac{\Sigma F_{Resisting}}{\Sigma F_{Sliding}} = \frac{R_v \tan(\delta) + B.L.c_w + P_p}{P_{sliding}} \tag{13}$$

where δ is the friction angle between the wall and the soil, c_w is the adhesion between the base and the soil and $P_{sliding}$ is the total sliding force.

2.5 Graphic Statics Application on Arches

Arches are one of the most common features of masonry constructions. Despite its outstanding strength in compression, masonry is assumed to have no tensile capacity. Therefore, each stone block in a masonry arch is under compression. The resultant of all the forces on individual voussoirs applied on the abutments is named as the thrust of the arch. Considering two voussoirs are acting against each other only at the resultant force location at the joint, connecting those points define the thrust line of the arch. Furthermore, Hooke revealed that in the case of an arch having voussoirs of the same size, like a cable, the thrust line is in the form of an inverted catenary [5].

The thrust line may have different configurations depending on factors such as the loading or the arch geometry, but every thrust line within the boundaries of the arch is considered to be a possible equilibrium solution. In other words, due to the thickness of the arch there are infinite possible thrust lines, making the arch a statically indeterminate structure. It is impossible to determine the actual thrust line of a stable arch, which is not necessary indeed. The Lower-Bound Theorem states that if the internal forces are in equilibrium with the external loads within the context of material assumptions, such as null tensile strength, the structure will not collapse. This is ensured if a thrust line can be determined within the boundaries of the structure, and the external load is said to be the lower-bound of the ultimate load that would cause failure. On the contrary, it cannot be concluded that the arch is

unsafe when a thrust line could not be located, unless all the infinite possibilities are checked by following a systematic approach.

By the contribution of several researches to the enhancement of Catenary Principle, a graphical method was developed to determine the possible thrust lines of an arch. There are three variables per arch, combination of which causes infinitely many thrust lines, namely the magnitude, position and the direction of the thrust at one of the ends. In order to initiate the graphic statics application on the arch, an assumption has to be made for one of those parameters.

First, the arch is discretized into a series of small voussoirs. Then, the forces acting on each voussoir are identified. The magnitude and direction of the resultant force is determined by the vectoral sum of the forces in the form of a force polygon. The components of the force polygon connecting each vector to an arbitrary location are used to construct the funicular polygon. By connecting each vector with its respective component from the force polygon, the funicular polygon is constructed. As it can be seen from Figure 13, the funicular polygon has a shape of a catenary. Therefore, by inverting the funicular polygon, the thrust line is determined. If it lies within the boundaries of the structure, the arch is deemed safe.

FORCE POLYGON

FUNICULAR POLYGON

(a)   (b)
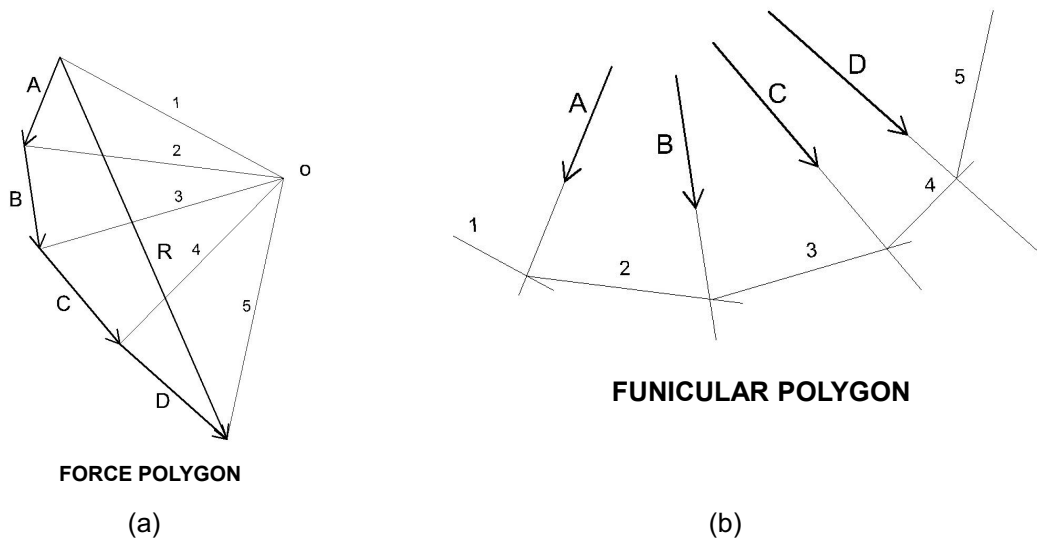
Figure 13. Graphic Statics application on arch (a) Force polygon (b) Funicular polygon[6]

2.6   Close Range Photogrammetry

Photogrammetry is a method of interpreting one or more images of an object to obtain its shape and location which is applicable to any object that can be photographed. The method can be used with the aim of creating a three-dimensional model of the object in a digital format or in a graphical format such as drawings or maps. The output model can be used to take measurements on the object or to obtain coordinates of points depending on the type of method used.

It can be divided into many categories based on the distance between the camera and the object, number of images allowed or the recording and processing methods. According to the first one, it can be categorized as Satellite, Aerial, Terrestrial, Close range and Macro Photogrammetry. Close range photogrammetry which stands for the cases where the imaging distance is less than 300 m, is a feasible non-contact measuring tool for existing structures.

There are several factors from the optical process that produces the image and the image acquisition procedure affecting the quality of the model. These involve the light sources, surface morphology of the object, the medium that the light rays travel in and the properties of the camera and the sensor. After capturing the images, interpretation and measurement methods recognize points of the object from their form, brightness and colour distribution. In addition to this information, the location of each point within the object is recorded. By using the available data, a mathematical transformation is applied from image to object space to reconstruct the object in a digital format.

The fundamental mathematical model of photogrammetry is central projection imaging. There are bundles of rays between each camera location and points in the object. Intersection of at least two spatially separated image rays locate a point in the space (Figure 14). [7]
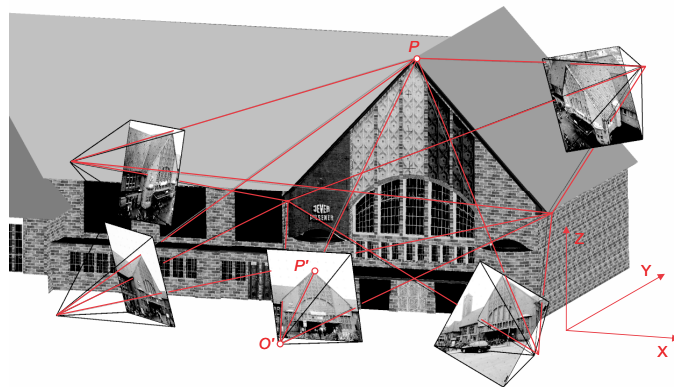
Figure 14. Locating a point by intersecting image rays from different camera locations [7]

This page is left blank on purpose.

3 AVAILABLE INFORMATION

3.1 Mur Casa Salvans Overview

Mur Casa Salvans is located in the northern section of Vallparadís Park in Terrassa, Spain. The wall was built in 1909 by the architect Lluís Muncunill i Parellada (Figure 15). It consists of two sections, the first one covers the area from the corner with Salmerón Street up to the turning point of the wall near the pedestrian bridge crossing Vallparadís Garden. This study is focused on the second section of the wall, that contains 11 arches of varying shape and dimensions, connected by buttresses (Figure 16)

Figure 15. An ancient photo of Mur Casa Salvans[8]
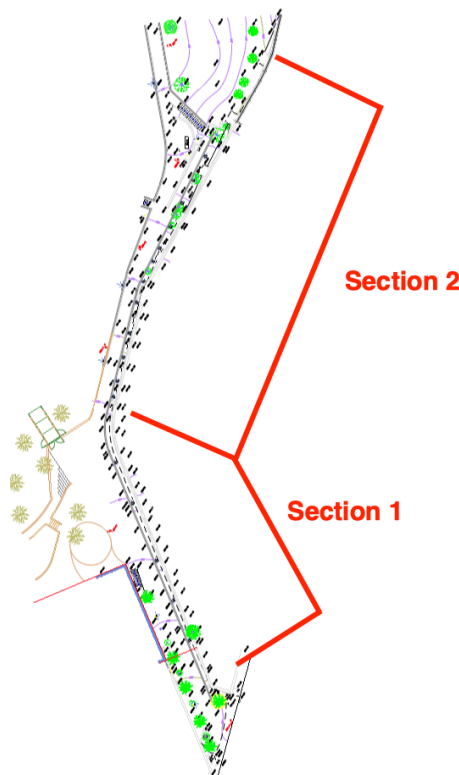
Figure 16. Plan View of Mur Casa Salvans

The height, the span and the thickness of the arches increase as one follows the descending slope of the adjacent path. The enumeration of the arches that is used throughout the study starts from the intersection of the two sections towards the end of Section 2, such that Arch 1 has the smallest dimensions while Arch 10 has the largest and Arch 11 is the half arch at the end. The buttresses are numbered according to the arches that they are connecting (Figure 17).
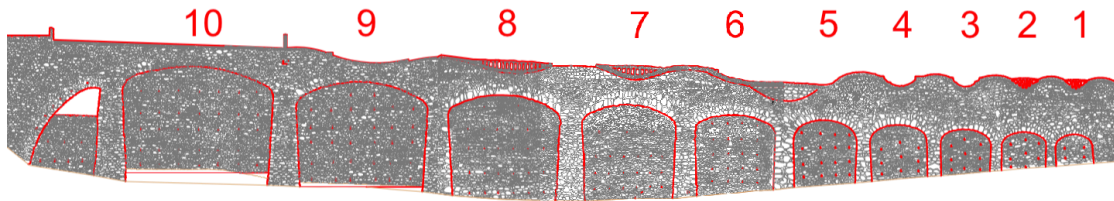
Figure 17. Enumeration of the arches in Mur Casa Salvans

The main body of the wall is composed of pebble stones bonded by mortar whereas the balustrades at the top of the wall are reinforced concrete ornamented by smaller sized pebble stones that accomplish a coherent appearance (Figure 18). Furthermore, there is a cantilever balcony made of reinforced concrete between Arches 5 and 6 where the direction of the road slightly changes (Figure 19).

| (a) | (b) |

Figure 18. Mur Casa Salvans (a) Arches 1-3 located in Section 2 (b) Section 1

Figure 19. The cantilever balcony section between Arches 6 and 5

Mur Casa Salvans has constantly changing inclination in both horizontal and vertical planes. It follows the slope of the adjacent road and the inclination of the wall with respect to the vertical plane changes as the size of the arches vary. Furthermore, the part of the wall below the arches have a bulging trend as the arch size increases (Figure 20). Thus, it is not possible to identify common vertical and horizontal surfaces applying to all models.

Figure 20. Arches 8 and 9 of Mur Casa Salvans

3.2   Topographic Survey

In order to determine the depth of the foundation, the dimensions and characteristics of the buried elements at the extrados of the arches and buttresses, a topographic survey was carried out by Terrassa Municipality. Initially, 22 pits of at least 0.75 × 0.75 m^2 size were proposed at the base of the wall located on the sides of the buttresses and at the top of the wall on the buttresses and the keys of the arches (Figure 21). However, Pit 9 at the base of Arch 7 and Pit 20 at the key of Arch 10 could not be excavated due to restrictions such as the presence of pipelines and the borders of a private property. The enumeration of the pits that was used in the initial proposal is used throughout the study (Figure 22).
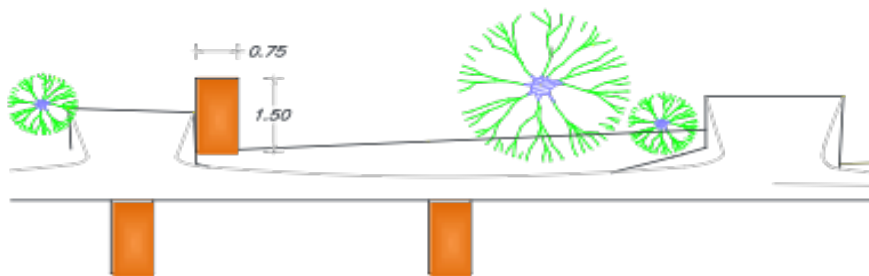
Figure 21. Positions of the pits
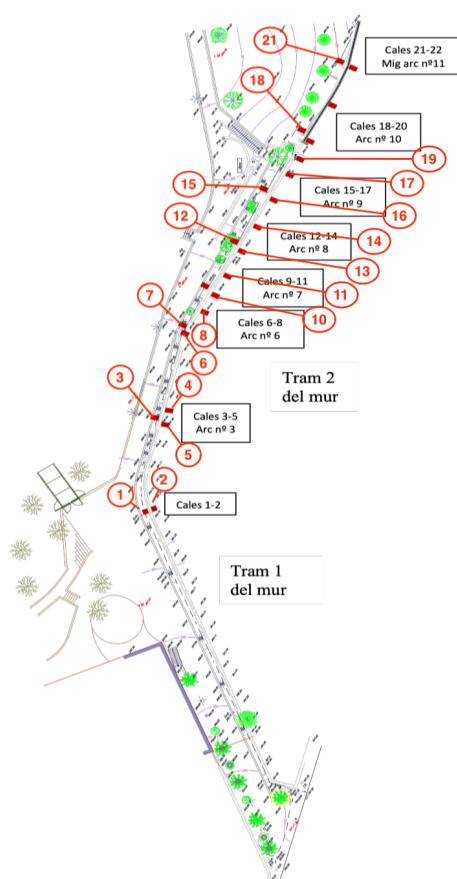
Figure 22. The pits performed on topographical survey of Mur Casa Salvans

The sizes of the pits were modified to assess the depth and width of the arches and the buttresses at the extrados. However, it was not possible to excavate up to the base of the wall due to the presence of buried pipelines or strong ground material and the limitation imposed by the adjacent road. The minimum excavation depth that was achieved is 75 cm at Pit 3 while at Pit 18 which is located on the buttress between the largest two arches, the depth of foundation could not be determined even after an excavation of 2.3 m. Furthermore, a steel rebar was driven to the ground at that location which could only move 50 cm deeper yet could not reach a different material that can be considered as an enlargement of the footing. In the pits at the bases of the buttresses of Arch 10, 9 and 8, concrete bases with enlarged widths were detected. For the pits located on top of the wall, the pit cross sections for the Pits 6 to 19 were provided by the municipality. In addition to the cross sections, measurements and photos taken during the survey for each pit are given in Annex.

3.3   Geotechnical Survey

At the request of Municipality of Terrassa, a geotechnical survey was carried out on May 2003 by the company Gesond S.A. Four boreholes of 14.5 m to 15 m were constructed on the area behind the wall in order to determine the soil profiles, characteristics of the sub-layers and the location of the water table. 9 standard penetration tests (SPT) were carried out at different layers and four samples were taken to be tested in the laboratory.

Three different layers were determined, of which the characteristics are tabulated in Table 1. Shear strength parameters, cohesion and internal friction angle, ϕ were obtained through correlations with SPT numbers of respective layers. At the time of the survey, the water table was located between 13.5 m to 14 m in all boreholes. Similarly, through SPT-N correlations, the bearing capacity of Layer A was determined as 0.14 MPa for rectangular footings of shallow foundations and the tip resistance of Layer B was determined as 2.45 MPa for deep foundations.

Table 1. Characteristics and Locations of Soil Layers [9]

Layer	Characteristics	Depth (m)	γ (t/m³)	c_u (kg/cm²)	Φ (°)
R	Filling material of sandy lime with gravel	0.8-1.2	1.8	0	24
A	Alluvial origin, sand slate and gravel with clay matrix	10-10.2	1.9-2.1	<0.1	30
B	Brown clay with sand and gravel, saturated from 13.5-14 m	10.2 -	2.1	0.3	28

3.4   Laser Scanning

Municipality of Terrassa provided elevation drawings obtained through previously performed laser scanning. The precise drawings of the front and back faces of the wall include elevations and provide useful two - dimensional information to be used in the following chapters (Figure 23 and Figure 24).
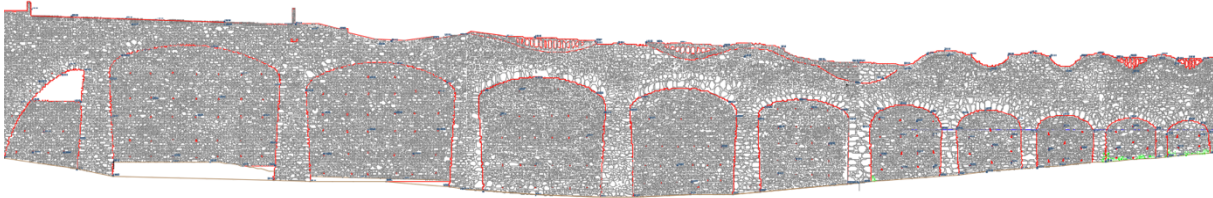
Figure 23. Elevation drawing of the front view
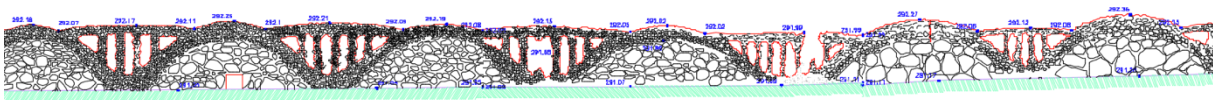
Figure 24. Elevation Drawing of Balustrades

4 PHOTOGRAMMETRY

4.1 Photogrammetry Survey

The photogrammetry survey of Mur Casa Salvans was performed on 12.04.2019 with the use of Canon EOS 600D digital camera with 18 megapixels resolution. The survey was carried out starting from Arch 10 and moving towards Arch 1. The larger Arches 8, 9 and 10 were surveyed individually. The size of the wall and the arches getting smaller towards Arch 1 enabled capturing several arches in the photos. Therefore, the surveys of Arches 5 to 7 and 1 to 4 were carried out together, respectively.

The camera settings were adjusted to obtain accurate photogrammetry models of the wall. To prevent any discrepancy between photos due to different zoom settings while still allowing enough coverage of the wall in each photo, the focal length was fixed at 18 mm. Consistent exposure was maintained throughout the surveys and ISO (light sensitivity) was set as low as possible to limit the noise in the photos, 200 in most of the cases. The F-stop number was calibrated to be as high as possible to have smaller aperture which results in a higher depth of field. Finally, the highest possible shutter speed was utilized to have sharper images that are required to produce accurate models.

For each model, photos were taken from different positions in an attempt to obtain overlapping images. Distance between the camera and the wall was maximized as enabled by the land, in order to focus a larger area of the wall and obtain better distance accuracy in the models. Any obstacle such as trees or lanterns were avoided from being captured as much as possible. However, the trees were leafing out since the survey was performed in spring. As a consequence, it was inevitable to avoid them especially in Arch 10, which has the highest plant population in front.

In order to scale and calibrate the models, at least 2 markers were placed with known distances on both sides of the buttresses and on the part of the wall below the arch for each individual arch (Figure 25). Furthermore, additional measurements were taken between identifiable locations in case of markers not being visible in some models.

Figure 25. Markers placed on the wall for scaling and calibration

Due to the inclination of the wall and the adjacent road, defining horizontal and vertical planes in coincidence with the wall was not possible. The markers on the buttresses were placed in such a way that a perfectly horizontal laser beam travels between them, which was verified by the level indicator of the laser distance meter. By this manner, the straight line between the markers on the buttresses will define the x-axis of the models.

Although it was not possible to follow a similar approach for the exact definition of the vertical plane, the inclination of the arches and buttresses with respect to z-axis were determined in a following survey. A plumb line, consisting of a metal ball and a string was used as a reference of a true vertical axis due to the action of gravity. It was hung down from top of the wall at the location of the buttresses and the keys of the arches, where accessible. Two points with a known vertical distance in between were marked on the string and the horizontal distances from them to the wall were measured. By the use of trigonometry, the angle of the section with respect to the z-axis was determined. In addition, the inclinations of the buttresses were measured with "iHandy Carpenter" mobile application at the locations that are reflective of the overall trend (Figure 26). [10]

(a)   (b)
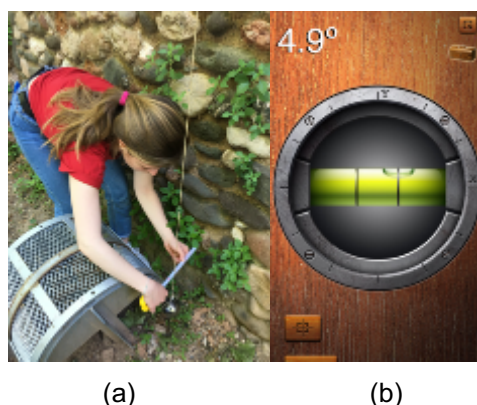
Figure 26. (a) Inclination measurement by (a) plumb line (b) Carpenter application

4.2   Photogrammetry Models

Using ReCap Photo, 3D photogrammetry models of the front of the wall were constituted. [11] The educational license of ReCap Photo allows to upload a maximum of 100 photos for a model. Due to this limitation, 4 separate models were created, namely Arch 10, Arches 8 and 9, Arches 5 to 7 and Arches 1 to 4 (Figure 27). The models were scaled and verified based on measurements taken on site and the mean error of all models is 0.90% (Table 2). Furthermore, accuracy of the models was also verified by comparing the arch lengths with the ones measured on the elevation drawings from laser scanning, yielding a difference of 0.51% (Table 3)
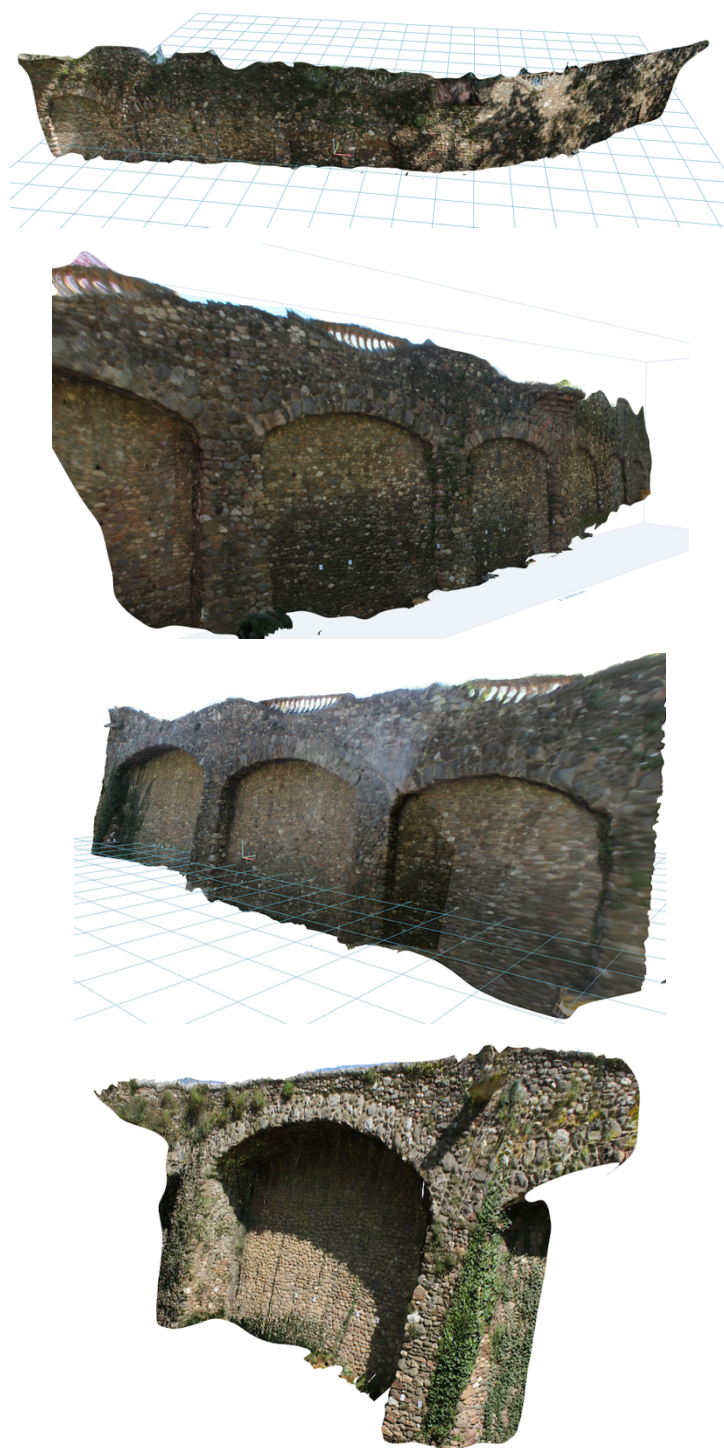
Figure 27. Models of Arches 1-4, 5-7, 7-9 and Arch 10 (from Top to Bottom)

Table 2. The comparison of the measurements taken on site and from the photogrammetry models

Arch	Measurement Number	Absolute Error (cm)	Error (%)	Mean Error (%)
10	1	2.8	2.86	
	2	2.2	2.20	
	3	3.18	2.54	
9	1	0.6	1.62	
	2	0.1	0.27	
	3	6.7	1.16	
	4	7.2	0.75	
8	1	0.8	0.10	
	2	5.3	0.54	
	3	1.4	0.15	
7	1	5.9	0.88	
	2	3.2	0.37	
	3	2.9	0.35	
	4	1	0.16	
6	1	1.3	0.23	
	2	0.24	0.21	
	3	6.4	0.87	
	4	2.8	0.40	
	5	1.9	1.76	0.90
	6	2.2	0.43	
5	1	1.55	0.34	
	2	5.7	1.08	
	3	4.4	0.79	
	4	0.2	0.19	
4	1	0	0.00	
	2	0.2	0.04	
	3	4.2	0.88	
3	1	3.9	1.04	
	2	0.4	0.49	
	3	12.9	3.24	
	4	1.8	0.48	
2	1	2.1	0.64	
	2	9	2.80	
	3	2	0.62	
1	1	2.6	0.96	
	2	2.5	1.74	
	3	1.7	0.97	

		4	0.4	0.14	

Table 3. Arch lengths measured from photogrammetry models and the drawing from laser scanning

Arch	Arch Length (cm)		Absolute Error (cm)	Error (%)	Mean Error (%)
	Photogrammetry Model	Laser Scanning			
10	1114.3	1110.9	3.4	0.31	
9	968.1	965.9	2.2	0.23	
8	805.4	821.3	15.9	1.94	
7	677.6	681.7	4.1	0.60	
6	563.4	563	0.4	0.07	
5	421.5	420.8	0.7	0.17	0.51
4	380.4	382.5	2.1	0.55	
3	348.5	348	0.5	0.14	
2	310.2	313.7	3.5	1.12	
1	241.6	241.6	0.0	0.00	

However, the models have some missing or blurry parts due to accessibility and visibility restrictions. As it was not possible to take aerial photos, the upper part of the wall, especially the balustrades, is the least accurate section throughout the models. Moreover, the plants in front of some arches and the elevation of the road resulted in missing parts at the bottom of the wall. Since the correspondence between laser scanning and photogrammetry was verified, the full height of the wall will be taken from laser scan data in the upcoming computations.

4.3   Sectioning Procedure

The safety of a retaining wall against overturning, sliding and base pressures can be assessed by appropriately analyzing representative cross sections. For that purpose, cross sections of the wall at different locations were constructed by combining the information about the front of the wall from photogrammetry models with the information from the topographic survey regarding the characteristics of buried elements.

The load pattern through the wall can be considered as from the key of an arch to the buttresses on side. As a consequence, a buttress takes loads coming from the halves of the two adjacent arches, becoming the most vulnerable structural element in terms of stability. Therefore, stability analysis has to be performed based on the failure of individual buttresses along with the adjacent half arches. Since every arch and buttress is unique in terms of dimensions and shape, assigning a single cross section to the unit, composed of the buttress and the arches, is not applicable. Therefore, 18 sections between the vertical axis of a buttress and the key of an arch were isolated from the models to assess

the stability of the wall in segments. In addition to these, several sections were extracted from the buttresses, keys of the arches and arbitrary locations at the bodies of the arches to evaluate the variation of dimensions and inclination of the wall. In this section, the sectioning procedure will be explained in detail.

4.3.1 Alignment and Mesh Decimation in ReCap Photo

As it was discussed earlier, during the survey, the markers on the sides of the buttresses were placed accordingly to provide a straight line in between, to be considered as the global x-axis. In order to adapt the same coordinate system orientation throughout the wall, the models were aligned in the same way in ReCap Photo using the "Orientation Tool". The grid lines passing through the markers were used to define the x-axis, to the right, y-axis is into the wall and z-axis is going up to the sky (Figure 28 and Figure 29).
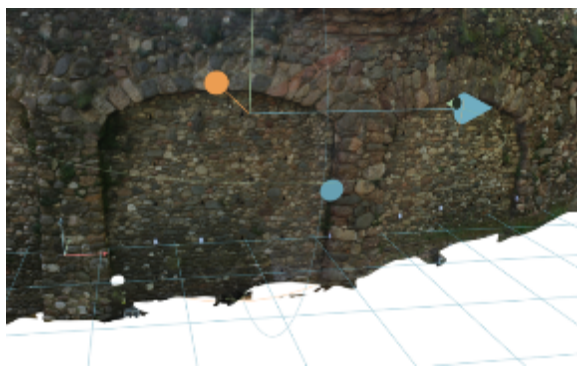
Figure 28.Gridlines passing through the markers defining the x-axis
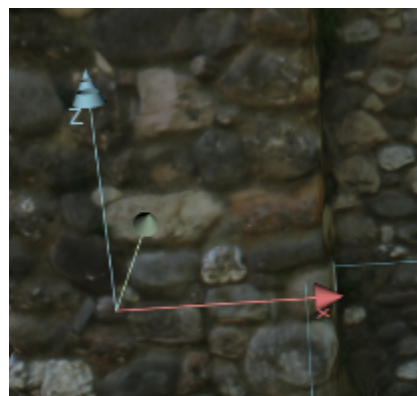
Figure 29.Global Coordinate System

In order not to alter the vertical inclination of the wall, the models were never rotated about the x-axis. In majority of the cases, the desired alignment was achieved by translation in x and z-axes and rotation about z-axis to have gridlines parallel to the wall.

In some cases where the change of inclination and direction of the adjacent road are more drastic, specifically in Arches 5, 6 and 7, the model was aligned to each of them separately in order to maintain the line between the markers horizontal. On the other hand, in the cases where the road has a milder slope and a constant direction, as in Arches 1 to 4, aligning the model to only one of them was sufficient in maintaining the horizontality of the gridlines for each arch.

In order to have better computational performance in the following steps of the analysis, the meshes were decimated to have 10.000 faces approximately. In order to maintain the accuracy of the geometry, "Best geometry" tool of ReCap Photo was utilized which results in the loss of textures. Then, the accuracy of the decimated sections was verified by comparing them with the original

meshes (Figure 30). Finally, the sections were exported in ".obj" format to be processed in CloudCompare. [12]
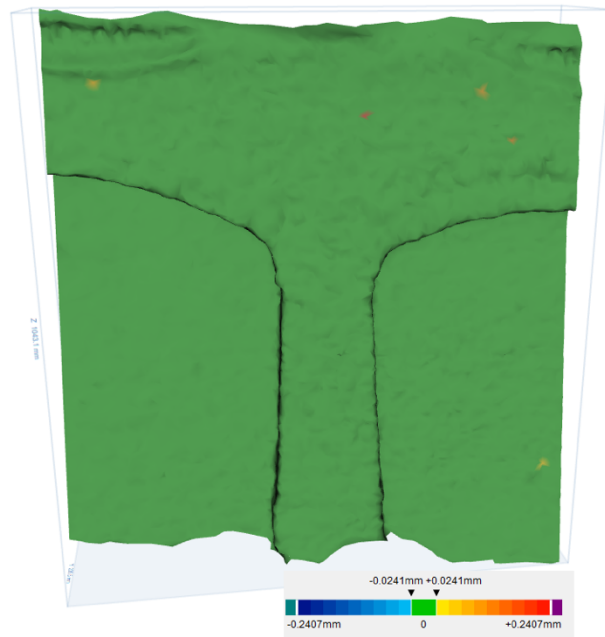
Figure 30. Comparison of the decimated section of Buttress 7-8 with the original mesh

4.3.2   Extracting Sections in CloudCompare

After the coordinate system was defined uniformly throughout the wall, the sections were extracted in CloudCompare. The bounding box that isolates a section from the model has the coordinate system pre-defined in ReCap Photo. However, due to the slope of the road, the box had to be aligned to obtain desired sections. The box was rotated about y-axis to have the z-axis passing through the key of the arch, resulting in sections cut by vertical planes (Figure 31). Similar to the alignment procedure in ReCap Photo, it was never rotated about x-axis to preserve the inclination of the wall.
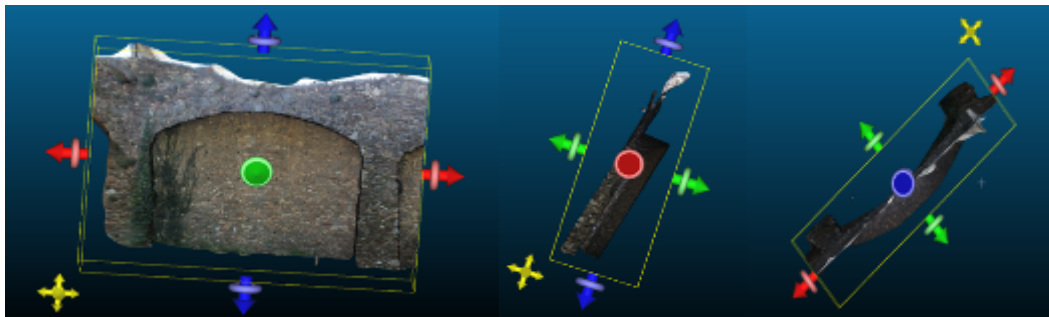
Figure 31. Front, top and side views of the aligned bounding box

The sections to be analyzed for stability, from the axis of the buttress to the key of the arch, were obtained (Figure 32). In order to evaluate geometrical variation, thin sections were extracted by setting

the bounding box width to 30 cm to avoid any deceptive irregularities (Figure 32).The sections were exported in ".dxf" format to be processed in AutoCAD. [13]
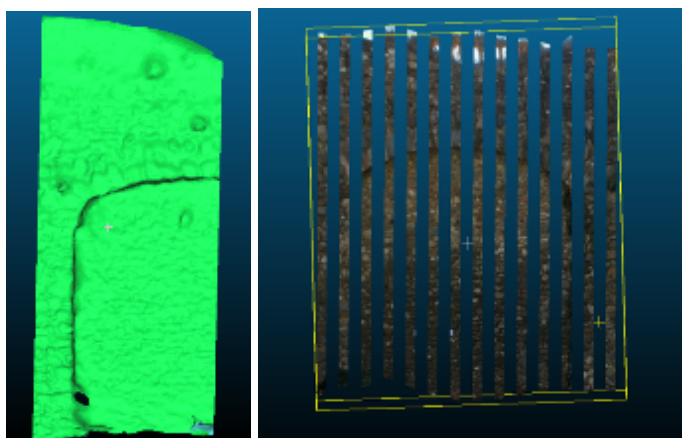
Figure 32. Sections of "Arch 6 with Buttress 7-6" (a) for stability analysis (b) for geometrical variation

4.3.3 Converting to 2D in AutoCAD

First, the section geometries were imported to AutoCAD. Since the stability analysis will be performed on the cross sections, the xy plane of the coordinate system was defined as the corresponding side view of the section. Then, the section was converted to 2D with the "FLATTEN" command to facilitate accurate dimensioning (Figure 33). Moreover, if the inclination of the resulting section was not matching with the inclination measurement taken on site, the section was rotated accordingly.

(a)   (b)
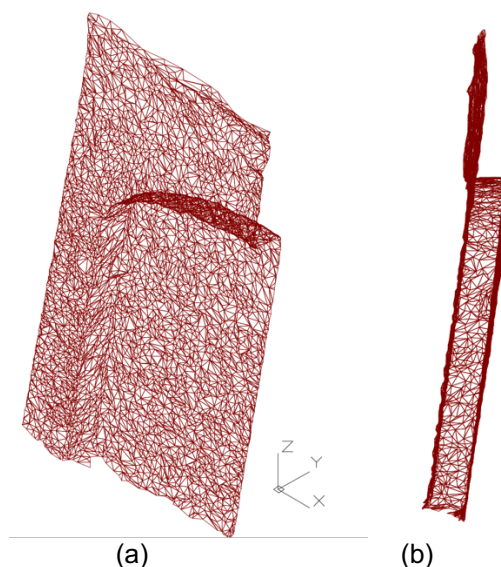
Figure 33. "Arch 8 with Buttress 9-8 "(a) before flattening (b) after flattening

4.4 Geometrical Variation

Sections of 30 cm thickness were obtained from CloudCompare to evaluate the variation of dimensions between arches and buttresses and also within individual arches. The sections are from the keys of the arches, the axes of the buttresses and arbitrary locations on the left and right side of the arch keys (Figure 34). Table 4 shows the heights of the sections obtained from the arches and buttresses. Mostly, the buttresses are higher than the parts of the wall with the arches. The height of the studied section of Mur Casa Salvans ranges from 6.16 m to 9.45 m. Arches 7 and 8 are the parts of the wall having the maximum height, which complies with the elevation view from laser scanning.
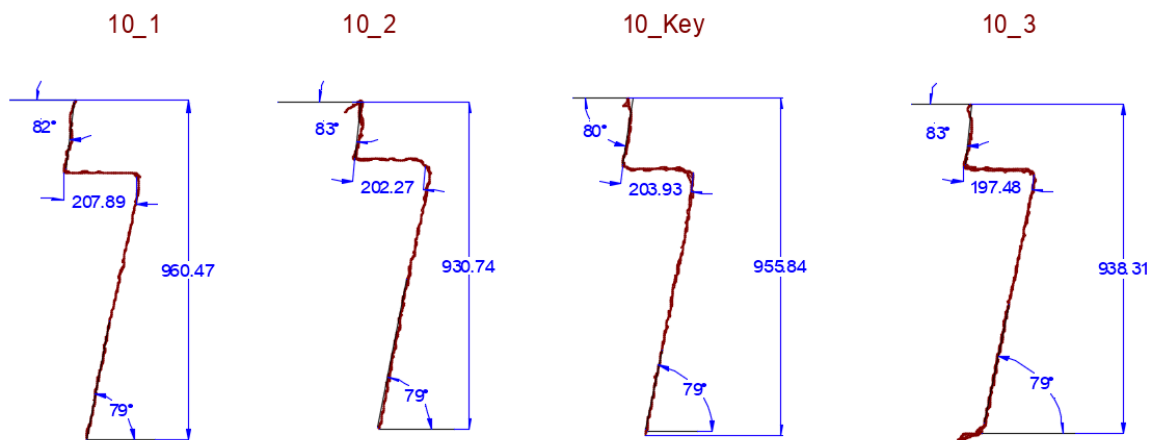
Figure 34. Sections from Arch 10

Table 4. The heights of the sections of the wall with the arch and the buttress

Arch	Height (m)					Mean Height (m)	Buttress	Height (m)
	Section 1	Section 2	Key Section	Section 3	Section 4			
1	-	6.22	6.22	6.05	-	6.16	1-2	6.34
2	-	6.63	6.52	6.37	-	6.51	2-3	6.69
3	7.19	6.48	6.70	6.34	6.68	6.68	3-4	7.14
4	7.53	7.47	7.23	6.91	7.12	7.25	4-5	7.60
5	7.82	7.23	7.44	7.29	7.05	7.37	5-6	7.75
6	9.11	8.83	8.60	7.97	7.72	8.45	6-7	9.58
7	9.73	9.95	9.95	9.92	9.74	9.86	7-8	9.37
8	9.75	9.88	9.72	9.77	9.91	9.80	8-9	9.51
9	8.69	9.03	8.66	8.74	8.89	8.80	9-10	9.91
10	9.60	9.31	9.56	9.38	9.38	9.45	10-11	9.58

Table 5 illustrates the top and bottom inclinations of the sections extracted from the arch keys and the bottom inclination of the buttresses. The inclinations do not vary drastically within an arch and since

the stability analysis was carried out on the sections between the keys and the buttresses, the angles of those were used in the upcoming calculations. The angle that the bottom of a section makes with the horizontal is of vital importance for overturning calculations as it affects the thicknesses to be used in volume calculations, and the moment arms of the weights of the section components. Smaller arches of Mur Casa Salvans are more vertical compared to the larger ones, as the inclination of the wall significantly reduces towards Arch 10. The angle between the top of the wall and the horizontal, measured counter-clockwise, was used while determining the thickness of the spandrel to calculate the volume of the corresponding section (Figure 34).

Table 5. Top and bottom inclinations of the wall at different locations measured from horizontal

Arch	Key Section		Buttress	Bottom Inclination (°)
	Top Inclination (°)	Bottom Inclination (°)		
1	87	86	1-2	86
2	86	86	2-3	85
3	88	87	3-4	86
4	85	84	4-5	85
5	86	85	5-6	85
6	84	84	6-7	84
7	85	83	7-8	86
8	86	82	8-9	81
9	82	81	9-10	79
10	80	79	10-11	79

As it can be seen from Table 6, the visible width of the arch increases significantly with increasing arch size. The thicknesses of the first four are compatible with each other while the thickness of Arch 10 is 10 times the first one. This trend validates it is quite possible that Arches 1 to 4 are constructed with decorative purposes and they are not functioning as structural arches.

Table 6. Exposed arch width of different arches measured at the highest point of the arch

Arch	Exposed Arch Width (cm)					Mean Thickness (cm)
	Section 1	Section 2	Key Section	Section 3	Section 4	
1	-	20.26	19.01	19.62	-	19.63
2	-	21.51	21.62	19.76	-	20.96
3	22.69	18.79	22.36	20.23	22.5	21.31
4	24.60	21.57	24.34	24.5	26.35	24.27
5	24.19	22.13	22.65	25.05	26.86	24.18
6	44.19	41.48	37.99	43.31	-	41.74
7	45.05	43.25	46.05	43.77	40.01	43.63
8	75.63	81.86	77.80	87.91	88.33	82.31
9	165.04	164.64	167.51	158.28	127.34	156.56
10	207.89	207.27	203.93	196.98	174.22	198.06

This page is left blank on purpose.

5   STABILITY ANALYSIS

As discussed in Section 4.3, stability of Mur Casa Salvans was assessed by analyzing the cross sections of the segments between the central vertical axis of a buttress and the key of the adjacent arch. The photogrammetry models provide 3D information about the front and the inclination of the wall. Previously performed laser scanning is a powerful tool on providing missing information about the visible parts of the wall, such as the full height. Moreover, the areas were obtained from the elevation drawing instead of the meshes from photogrammetry models. Since it was validated earlier that laser scanning conforms to photogrammetry models, calculating areas from the elevation drawing is less demanding in terms of computational power while preserving the accuracy of evaluated areas. Finally, the information about the buried parts of the wall was gathered from the topographic survey, such as the foundation dimensions, arch width, thickness and its location relative to the ground level. By combining the sections extracted from the photogrammetry models with the information about the back of the wall, several cross sections were constructed for the stability analysis.

Figure 35 shows the section between the keys of Arches 7 and 6 in 3D in which there are two sections to be analyzed for stability, divided by the axis of the buttress. When the exact data from topographic survey was merged with the meshes of the wall from the models, three different cross sections were obtained for the keys and the buttress, respectively (Figure 36). As it was discussed in Section 4.4, the configuration of the front of the wall varies significantly from the key of an arch to the key of the adjacent one, which is also true for the back of the wall. These variations combined with different alignments of the arches, especially in larger ones, obliged to divide the sections at the buttress axis and analyze them separately. Furthermore, due to these variations and the uncertainties on the characteristics of the buried elements, some assumptions had to be made to simplify the sections to proceed to two -dimensional stability analysis.
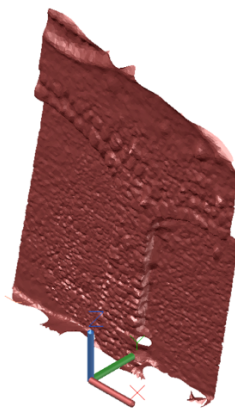
Figure 35. 3D view of a section between the keys of Arch 6 and 7
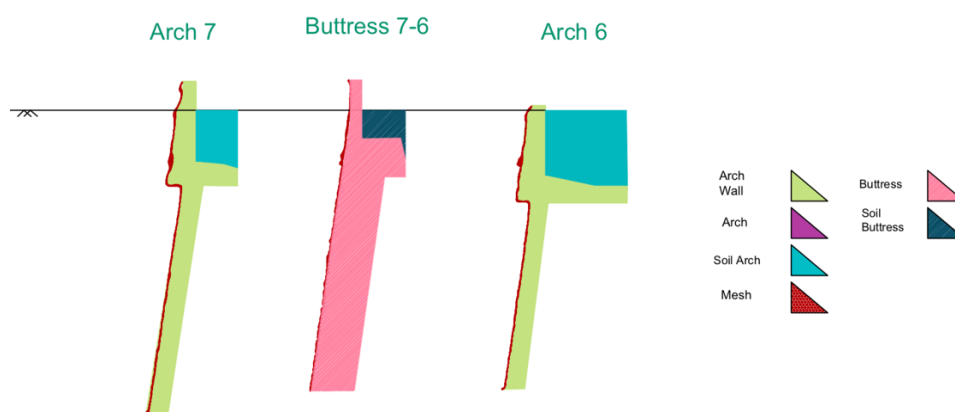
Figure 36. Cross sections of the key of Arch 7, Buttress 7-6 and Arch 6

The legend that was used in AutoCAD drawings to distinguish between different sections are tabulated in Table 7. All components located within the boundaries of the buttress, namely the buttress itself, buttress foundation and the soil mass above buttress were represented in hatched areas. The sections within the wall with the arch have solid areas and when two sections overlap, those areas were represented in gradient colors of the components.

Table 7. Legend of colors used in AutoCAD drawings

Section	Representation
Mesh	Red
Wall with arch	Green
Buttress	Pink - Hatched
Buried arch	Purple
Soil mass above arch	Blue
Soil mass above buttress	Navy- Hatched
Arch Foundation	Dark Green
Buttress Foundation	Dark Green - Hatched

5.1 Assumptions

5.1.1 Soil Layers and Soil Parameters

The soil profiles between the boreholes S1-S2 and S3-S4 provide an insight about the existing soil layers behind different sections of the wall. Borehole S1 is located at Section 1 which is beyond the scope of this study while S2 is located behind Arch 1, S3 is aligned with Arch 6 and S4 is located behind Arch 9 (Figure 37). Although none of the profiles intersect the wall, the locations of the layers were estimated by overlaying the profiles with the front view of the wall and matching the elevations. In Arches 6-10, the wall is mostly in contact with Layer A followed by Layer B at the bottom. The height of Layer B increases towards Arch 10. For Arches 1-5, it can be assumed that Layer A is prevalent throughout the wall height. (Figure 38)
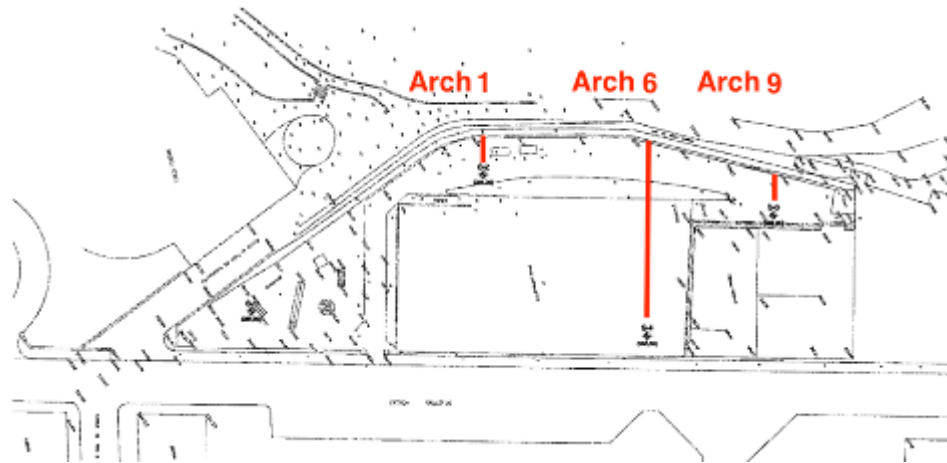
Figure 37. Locations of the boreholes with respect to the arches
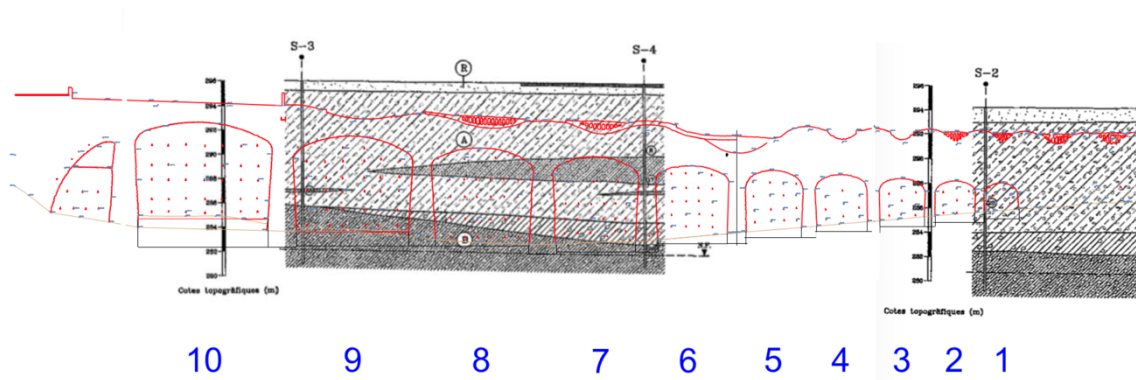
Figure 38. Soil profiles overlaid on the front view at corresponding elevations

For Layer A, the specific weight was assumed to be 20.6 kN/m^3, the upper bound of the range provided by the geotechnical survey and the friction angle, φ was taken as 30°. The undrained cohesion was specified as smaller than 0.1 kg/cm^2. To calculate the earth pressures in a conservative manner and to facilitate the application of Coulomb's Theory of Lateral Earth Pressure by ignoring the tension crack development, the cohesion was neglected except for sliding calculations. c_u was taken as 0.1 kg/cm^2 to provide adequate shear resistance as the wall is significantly vulnerable to sliding as will be discussed later in Section 5.3. Although it can be suggested that Layer B exists at the bases of Arches 6-10, it was not possible to estimate the depth of the layer in contact with the wall. Owing to the fact that the two layers have the same specific weights and relatively close friction angles, assuming Layer A for the full height of the wall was adequate. For Arches 6-10, Layer B was assumed at the level of foundation bases.

From the elevation view, the bottom of Buttress 7-8 is the deepest point of the wall above ground, with a depth of 9.7 m, measured from the ground level behind the wall. The water table was located at 13.5

– 14 m which is far below the wall. Therefore, due to the absence of pore water pressure, the effective stress is equal to the normal stress throughout the wall.

Conservatively, the internal friction angle between wall and soil, δ was assumed to be the half of the friction angle, φ as the lower bound of the recommended range. Due to small undrained cohesion values of the layers, assuming the wall adhesion, c_w, equal to c_u was deemed as appropriate.

5.1.2 Materials

Masonry was assumed to prevail throughout the wall, with a specific weight of 22 kN/m³ as suggested by NTC 2008, Italian National Seismic Code for rectangular masonry stone blocks [14]. The exceptions were the reinforced concrete balcony section between Arches 5 and 6 and plain concrete at the bases of the Arches 8,9 and 10. As the amount of reinforcement in the balcony is unknown, it was neglected in the weight calculations. For those sections, the specific weight of concrete was taken as 24 kN/m³ for normal weight concrete [15].

5.1.3 Foundation

For the buttresses of Arches 8,9 and 10, the measurements of foundations taken on site were available. During the topographic survey, the pits were located on the left side of the buttresses except Pit 21, located on the right side of Buttress 10-11, since Arch 11 on its left side was filled with masonry. Therefore, the measurement taken on the left side of a buttress was used to define the level of foundation throughout the buttress. For the arches, the foundation was assumed to be at the same level as the one of the adjacent buttress' with the shallower foundation (Figure 39). For the arches 1 to 7, where there were no available measurements or the excavations had to be stopped due to land restrictions, foundation depth was assumed to be 80 cm measured from the left side, which is the shallowest foundation depth measured. The similar trend was assumed for the foundation of the arches.
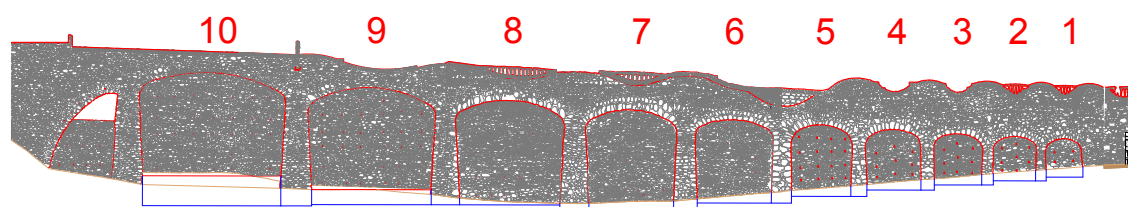
Figure 39. Assumed foundation configuration

The foundations of all sections were assumed to have rectangular cross sections. Concrete bases were used for Arches 8,9 and 10 as determined on site. While for the remaining arches that the

characteristics of the foundations remain unknown, the material of the foundation was assumed to be masonry with $\gamma = 22 \ kN/m^3$ as the wall. At the bases of the large arches, approximately 35 cm of enlargement was measured at the toe. Considering the common construction practices of foundations, it was deemed as appropriate to assume the same enlargement at the heel of the base. Similarly, two-way enlargement of 35 cm of was applied to the bases of Arches 1-7. Both of the assumed front and rear enlargements were implemented in the calculations as inputs that can be modified if necessary. Figure 40 illustrates the plan view of the assumed foundations from the key of Arch 8 to Arch 7 with the exact alignment.
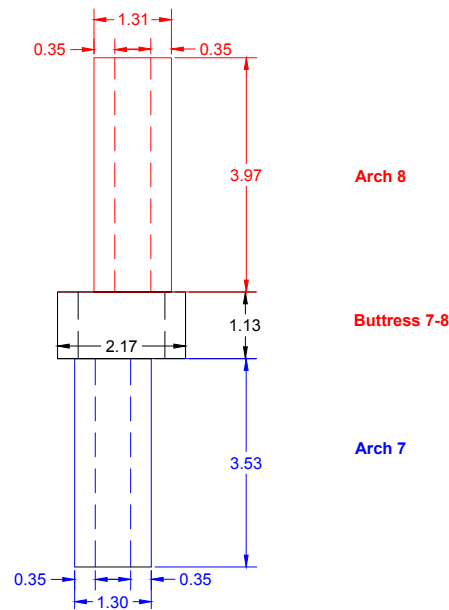
Figure 40. Plan view of Arch 7, Buttress 7-8 and Arch 8 foundations

5.1.4   Back of the Wall

During the survey, the parapet width was measured as 40 cm and the upper part of the wall exposed during the excavations was vertical. Therefore, vertical back face was assumed until the arch level throughout the wall. For the Arches 6 to 9, the ground level was determined from the topographic survey measurements. For the Arches 1 to 5 and 10 whose measurements were not available, the ground level was determined from the elevations obtained from previously performed laser scanning on the extrados of the wall.

5.1.5   Arches 5-10

The depths of the arches were determined from the topographic survey and modified to match the arch level at intrados if required. The cross section of the arch was assumed to be a rectangle (Figure 41).
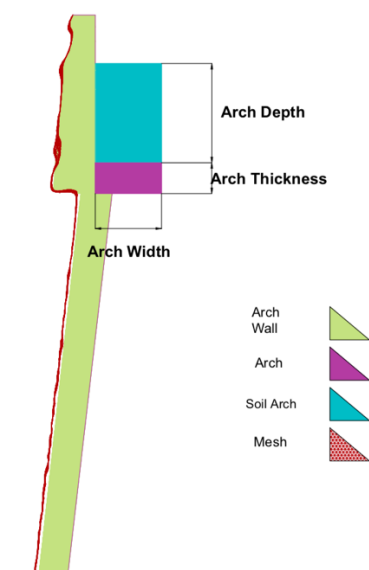
Figure 41. Assumed geometry for the arch of section "Arch 8 with Buttress 7-8"

For Arches 6 to 9, the arch widths and thicknesses were determined during the topographic survey. The measured thickness of 55 cm was assumed for Arches 5 and 10 too. Arch 6 has the largest arch width measured on site which is reasonable considering the additional load of the balcony section located on its buttress. The largest arch width for an arch without the balcony on the buttress was measured at Arch 8 as 2.11 m. For Arch 10, the arch width was assumed to be 2.1 m, a value that is close to the largest measurement of the arches with similar features and sustains a similar difference between consecutive arches of this section of the wall (Table 8). Arch 5 is one of the two arches that share the load of the balcony on the Buttress 5-6. Therefore, its width was assumed to be compatible with the width of its accompanying neighbour, Arch 6, but shorter due to the change of direction of the wall at that location. Figure 42 shows the plan view with arch widths for Arches 5 to 10, where the assumed widths are represented by red lines.

Table 8. Assumed arch widths

Arch	Width (m)	Difference (m)
10	**2.1**	-
9	1.85	**0.25**
8	2.11	0.26
7	1.54	0.57
6	2.66	1.12
5	**2.45**	0.21
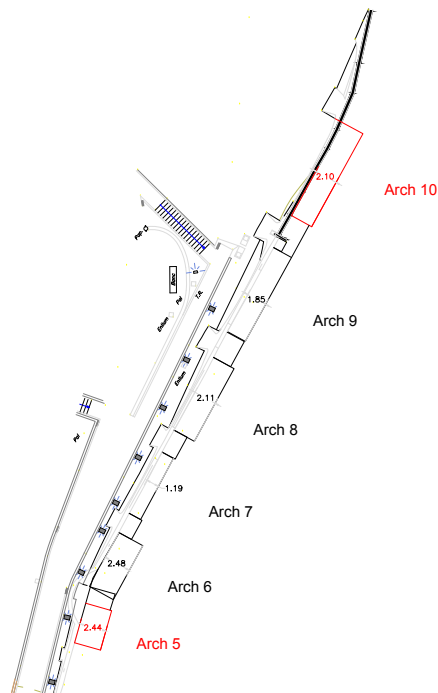
Figure 42. Plan view with arch widths for Arches 5-10

The shape of the back of the wall below the arch level was completely unknown. On site, the wall thickness was measured as 60 cm in several locations through drainage holes (Figure 43). Therefore, the wall thickness inside the soil was assumed to be 60 cm throughout the wall and the shape was assumed to be parallel to the front of the wall, to be conservative.

Figure 43. Drainage holes that enabled measuring the wall thickness

The rear edge of the buttresses was assumed parallel to the front until the level of the top of the adjacent arch, resulting in thick parallelogram cross sections. Additional to the visible thickness of the buttress, conservatively, the thickness inside the soil was taken as the same as the wall thickness, 60 cm. Above the thick partial cross sections, thin sections with vertical back face and previously defined parapet width were assumed together with soil on top of the lower section, until the ground level. The additional masonry area of the buttress above arch level was ignored for simplicity of the calculations and to have a conservative approach. Figure 44 shows the assumed cross section of Buttress 7-8.
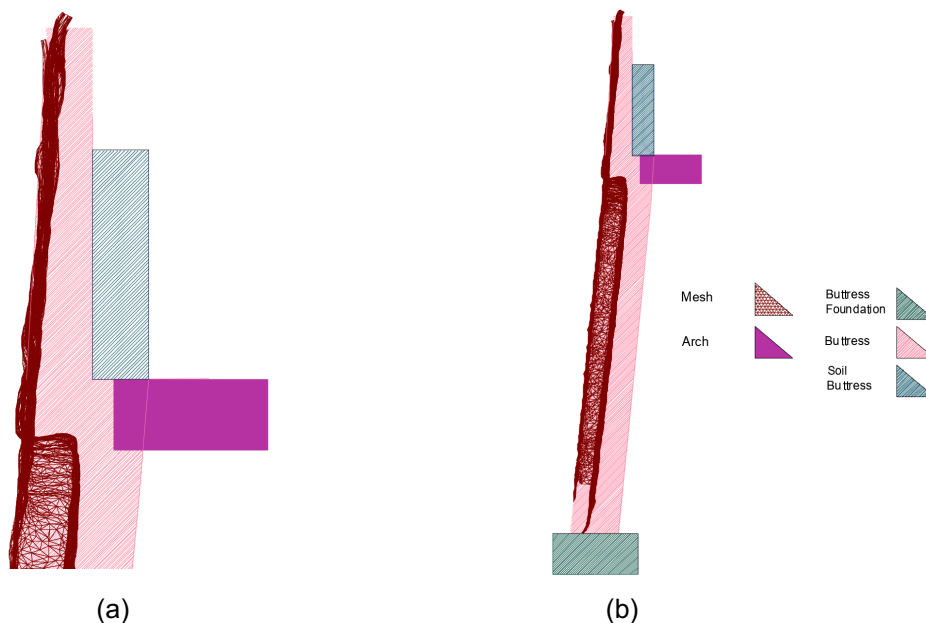
Figure 44. Buttress cross sections of " Arch 8 with Buttress 7-8" (a) above arch level (b) full height

5.1.6   Arches 1-4

Since Arches 1-4 are significantly smaller than the ones discussed above, these arches were assumed to be non-structural elements that were constructed to complement the coherent appearance. Therefore, for both of the arch and buttress, the back of the wall was assumed to be parallel to the front with a thickness of 60 cm inside the soil, up until the ground level. Likewise, there is the parapet of 40 cm width with a vertical back face, above the ground level (Figure 45).
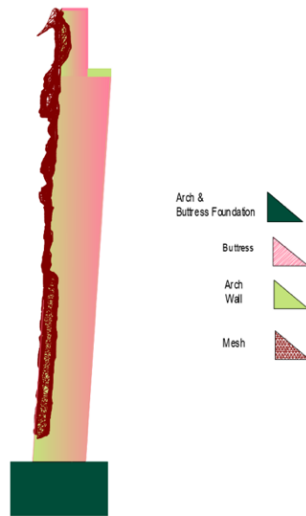
Figure 45. Assumed cross section of Buttress 2-3 with Arch 2

5.1.7 Cantilever Balcony

The reinforced concrete balcony section on Buttress 5-6 extends from the axis of the wall with a shape of a quarter ellipsoid. The shape and dimensions of the support extending towards the soil were unknown. In order to simplify the calculations, the balcony section was assumed to be a cone with an ellipse base, half of which is extending outside the wall while the other half supports the cantilever (Figure 46).

(a)   (b)
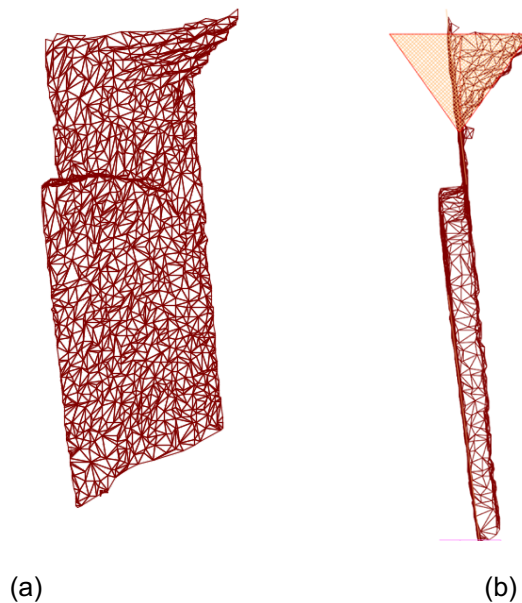
Figure 46. Half of the balcony at Buttress 5-6 (a) actual shape (b) assumed cross section

5.1.8 Surcharge Pressure

In the design of modern retaining walls, application of minimum 10 kN/m^2 surcharge pressure on the soil surface behind the wall is recommended. [4] The area behind the wall which is between the wall and Salmerón Street is highly accessible and there is even a sports court within this section. Based on that reasoning, surcharge pressure of 10 kN/m^2 was applied on the soil surface above the arch and the buttress. Since the ground level is inclined, the pressure was applied on the horizontal projection of the soil surface behind the wall.

5.1.9 Calculation Assumptions and Procedure

The forces acting on a cross section of the retaining wall are the weight of the structure, the weight of soil above arch level, surcharge on soil surface and its horizontal component, total active thrust and total passive resistance. The soil behind the wall was assumed to be in active case while passive case was assumed at the front of the wall. The forces due to lateral earth pressures were calculated by using Coulomb's Theory of Lateral Earth Pressure. Therefore, the total active thrust acts on the soil wedge at an angle δ below the normal to the wall while total passive resistance is applied on the soil wedge on front at an angle δ above the normal. Figure 47 illustrates the resultant forces and pressures acting on the cross section.

Figure 47. Schematic of forces acting on a cross section

The active thrust makes an angle of θ with the horizontal, which is illustrated in Figure 48, while passive resistance is has an angle of δ as a consequence of rectangular foundation assumption.
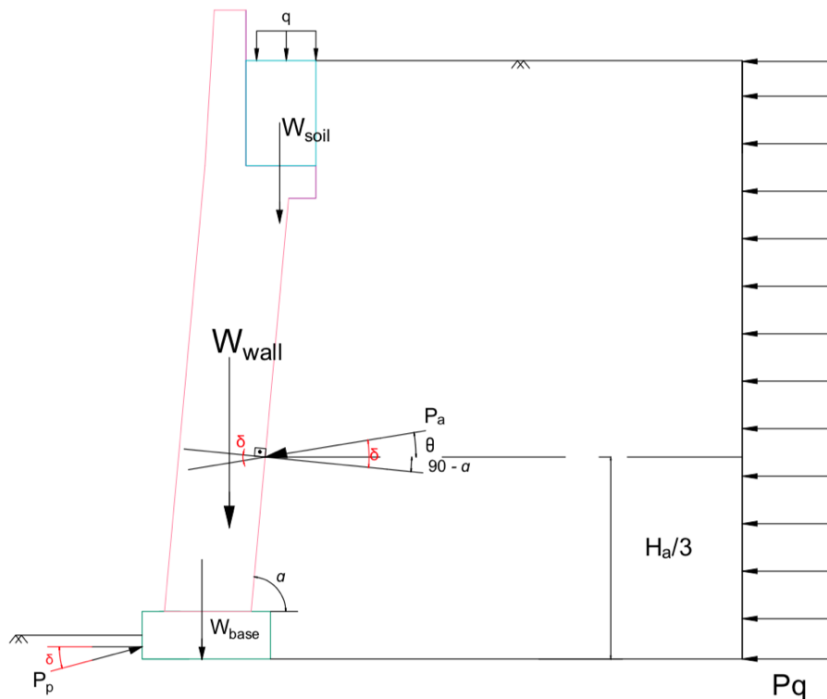
$$\theta = \delta - (90 - \alpha)$$

where α is the angle of the back face of the wall.
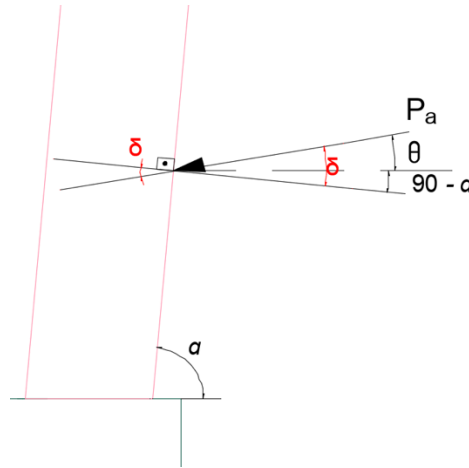
Figure 48. Derivation of the angle θ that P$_a$ makes with horizontal

For most of the cases, the back face of the wall and the arch sections have the same inclination, if not, the difference is in the range of 1-2°. Therefore, the buttress inclination was assumed throughout the section to compute the angle of the active thrust.

In order to assess the stability of each unit section, its weight and the moment about the toe of the foundation have to be determined. Although the buttress and the arch have their own bases with different dimensions, the unit section was assumed to behave monolithically as a consequence of the load path from the arches to the buttresses. Therefore, stability of the unit section against overturning was analyzed about the toe of the buttress foundation.

Due to the change of material, shape and inclination, the section was divided into smaller parts. The weight and the moment arm of each segment were obtained separately. For Arches 5-10, the section was divided into at least 8 parts, namely upper and lower sections of the arch wall, upper and lower sections of the buttress, extension of the arch towards the soil, soil masses above the arch and the buttress, the foundations of the arch and the buttress (Figure 49). The front view of the unit section with assumed foundation was used to obtain the areas of those segments, which was later converted to volumes by multiplying with the thicknesses measured in the cross-section view.

Figure 49. Areas of "Arch 9 with Buttress 9-8"

In the front view, the arch with 55 cm thickness perpendicular to the bottom line of the arch was drawn referring to the area of the arch extension inside the soil. The thick lower section of th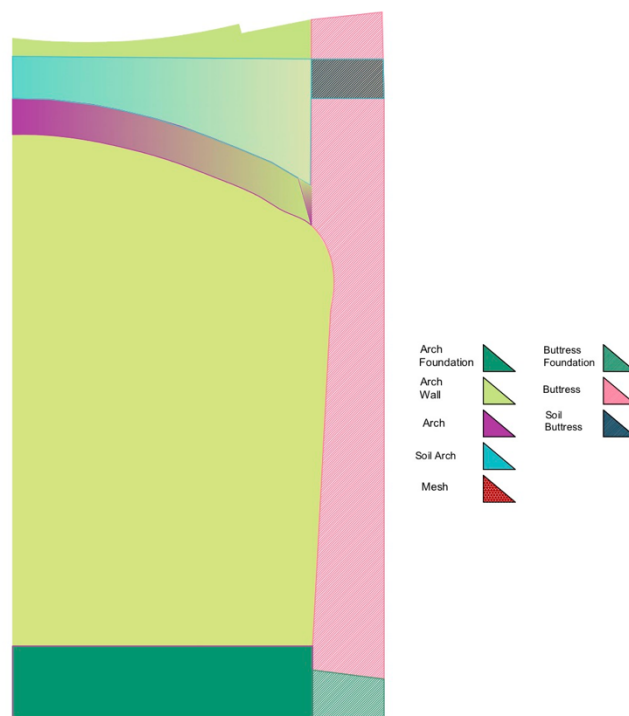e buttress was defined to be aligned with the top of the arch. Above that level, there is soil until the ground level as determined in topographic survey. The ground level and thus the height of the soil above the key of the arch were also known from the survey. The ground level was assumed to be linear between the key of the arch and the buttresses, defining the soil mass above the arch. After locating the origin at the toe of the buttress foundation, areas and centroids of the sections were obtained using the "MASSPROP" command.

In the side view, first, the height of the unit section obtained from the photogrammetry model was compared to the respective height in the front view. If required, the section was elongated to have the correct height. Since the pits at the top of the backfill were located at the arch keys and at the middle of the buttresses, the assumed cross sections refer to the left and right ends of a unit section. In the majority of cases, the top and bottom lines defining the wall are varying throughout the unit section. As a consequence, defining the arch and buttress ends at the top or bottom of the flattened cross section was challenging. As an alternative, the cross sections of the arch key and buttress were constituted separately by utilizing the thin slices extracted from the models at those locations. Then, the cross sections were placed on the side view of the unit section at their accurate locations by matching the meshes (Figure 50).
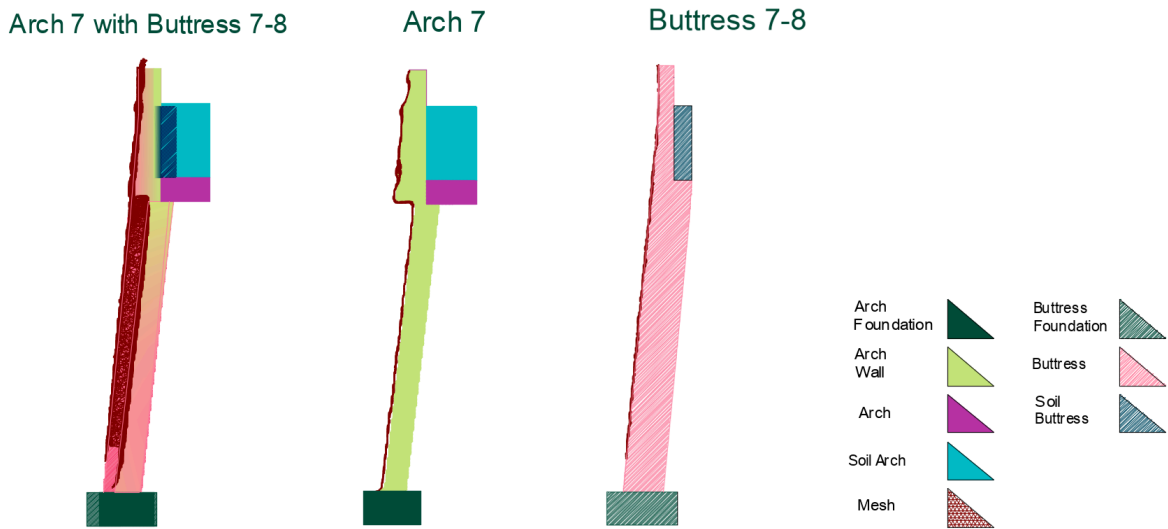
Figure 50. Cross sections of" Arch 7 with Buttress 7-8", Arch 7 and Buttress 7-8

The volume of each section was calculated by multiplying the areas obtained from the front view by the thicknesses on the side view. Due to their inclinations, the partial cross sections of the buttress and the wall below the arch are parallelograms. Thus, for the upper and lower sections referring to these parts, the thicknesses used for computing volumes were obtained by multiplying the horizontal thicknesses by the sine of the corresponding angle (Figure 51). After the volumes of each section were determined, the weights were calculated by multiplying each volume by the respective specific weight of the material for each segment (Figure 52).
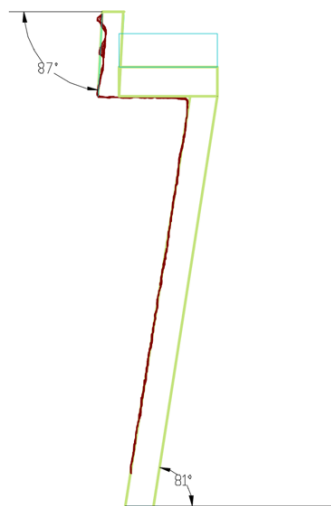
Figure 51. The angles used for determining parallelogram thicknesses
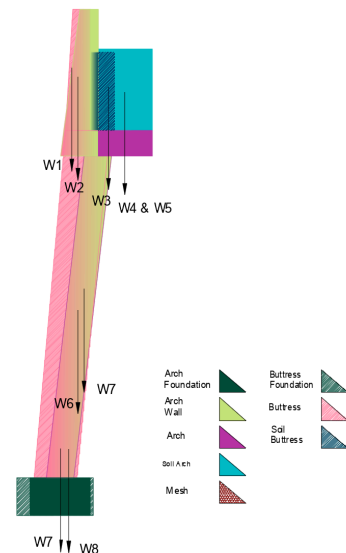
Figure 52. The weights of different segments of the cross section

When the origin is located at the toe of the buttress on the side view, the moment arm of any section refers to the x-coordinate of the centroid. From the front view, the y-coordinate of the centroids, $\bar{y}$, were already determined. The centroid of a section was determined by drawing a horizontal line $\bar{y}$ distance above the origin and intersecting it with the centerline of the section. By this manner, the x-coordinate of the centroid, $\bar{x}$ thus, the moment arm was determined (Figure 53).
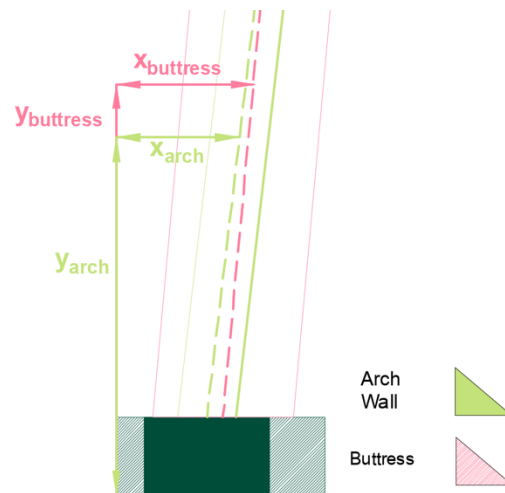
Figure 53. Determination of the moment arm of the inclined elements of the wall

5.2   Procedure

The ground level behind the wall, which was used in the active pressure calculations, was taken as the ground level at the middle of the section (Figure 54). During the topographic survey, pipelines were located at 40 cm depth from the ground at Section 1 and the highest pit of Section 2, located on Buttress 2-3. Since the passive pressure is not acting on the wall where there are pipelines, the line defining the ground level was assumed to be 50 cm lower than the actual ground level for the passive pressure calculations. Then, the centerline of the remaining foundation area was used to define the soil height for passive pressure (Figure 55).
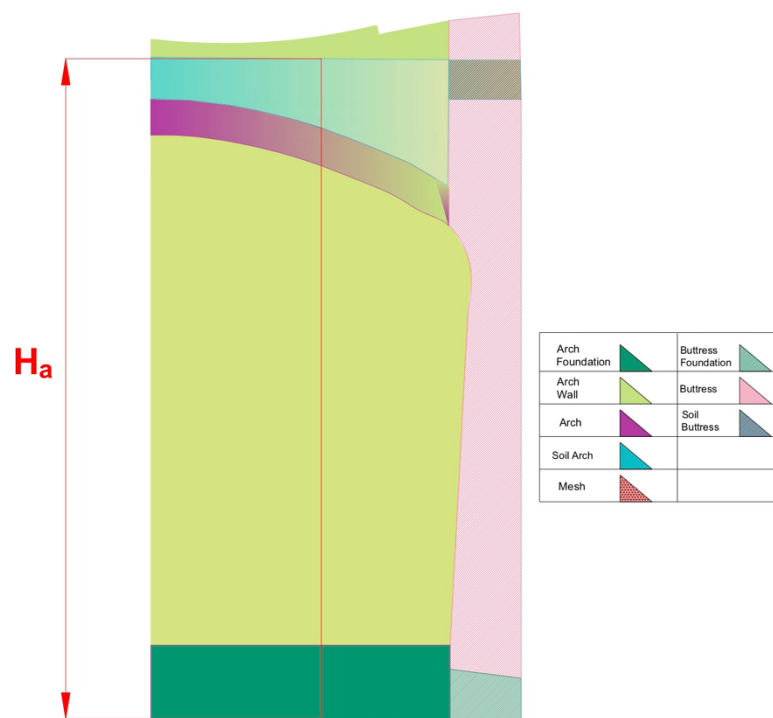
Figure 54. Active Pressure Height Assumption
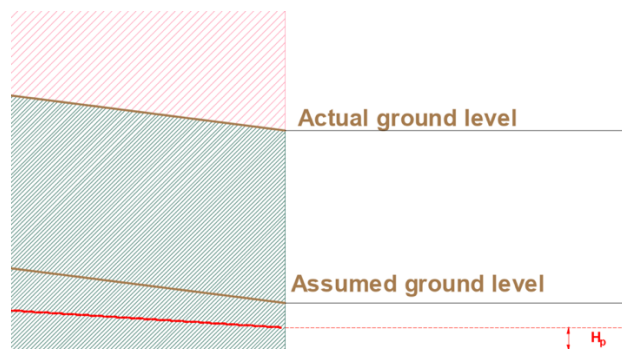
Figure 55. Passive Pressure Height Assumption

The active and passive pressure coefficients were calculated by using equations (5) and (7) for each section with their respective back face angles. Although Coulomb's Theory does not provide lateral earth pressures, it enables the assumption of triangular pressure distribution. Therefore, the total active thrust and the passive resistance over the length of the wall were calculated as follows.

$$P_a = \frac{1}{2} \cdot \gamma \cdot H_a^2 \cdot K_a \cdot L$$

$$P_p = \frac{1}{2} \cdot \gamma \cdot H_p^2 \cdot K_p \cdot L$$

where H_a and H_p are the assumed active and passive pressure heights and L is the length of the wall.

Then, the horizontal and vertical components of the earth pressures were obtained as

$$P_{a,h} = P_a \cdot cos\theta \qquad\qquad P_{a,v} = P_a \cdot sin\theta$$

$$P_{p,h} = P_a \cdot cos\delta \qquad\qquad P_{p,v} = P_p \cdot sin\delta$$

where θ is the angle described in Figure 48.

Since both forces are the resultants of the triangular pressure distributions, they are applied to the wall at H/3 of the respective heights. The moment arm of the vertical component of P_a was calculated as follows (Figure 56).

$$\bar{x} = e_{front} + t_{buttress} + \frac{H_a/3 - h_{foundation}}{tan\alpha}$$

where e_{front} is the enlargement of the footing at the toe, $t_{buttress}$ is the buttress thickness, $h_{foundation}$ is the foundation height and α is the back face angle.

Figure 56. Moment arm of the vertical component of P_a

The assumed surcharge on the soil surface behind the wall causes a constant lateral pressure on the wall. The resultant force of this pressure has a moment arm of $H_a/2$ and was calculated as follows

$$P_q = q.K_a.H_a.L$$

where q is the surcharge pressure.

After all the forces and the moment arms with respect to the toe of the buttress foundation were obtained, the factor against overturning was determined as the ratio of the stabilizing moments to the overturning ones.
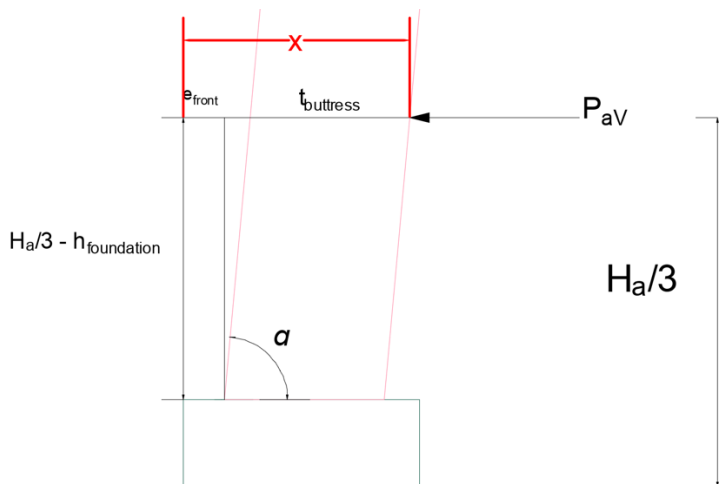
$$F_{overturning} = \frac{\Sigma M_{Stabilizing}}{\Sigma M_{Overturning}}$$

Similarly, the factor against sliding was determined as the ratio of the sum of the sliding forces to the sum of the resisting forces.

$$F_{sliding} = \frac{\Sigma F_{Resisting}}{\Sigma F_{Sliding}}$$

For the particular case of Mur Casa Salvans, the wall adhesion, the wall friction and the passive resistance resist sliding while the horizontal components of the active thrust and the surcharge are the sliding forces. Considering the different base widths of the arch and buttress foundations, the factor against sliding might be expressed as

$$F_{sliding} = \frac{c_w.(B_1 L_1 + B_2 L_2) + R_v.\tan(\delta) + P_p}{P_{A,h} + P_q}$$

In order to evaluate the effect of the adhesion between the wall and the soil, the factor against sliding was also calculated neglecting c_w.

If the overturning criteria was satisfied, the base pressures were calculated based on the eccentricity case, as discussed in Section 0. The location of the resultant force was determined by dividing the net moment by the vertical component of the force. As discussed earlier, the section is expected to move monolithically about the toe of the buttress foundation. Therefore, the eccentricity of the resultant force with respect to the centerline of the buttress base was determined. However, since the base width of the arch foundation is smaller than the one of the buttress, using the latter along the entire section length would underestimate the base pressures by providing a larger area. Therefore, the mean base width was used in the upcoming calculations for base pressures (Figure 57).
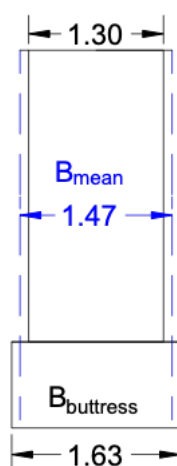
Figure 57. The base width assumption for base pressure calculations of "Arch 6 with Buttress 5-6"

For small eccentricity of e ≤ B/6, the maximum and minimum base pressures were calculated as follows

$$\sigma_{max,min} = \frac{R_v}{B_{mean}.L_{total}}\left(1 \pm \frac{6e}{B_{mean}}\right)$$

When e > B/6, the maximum base pressure was calculated as

$$\sigma_{max} = \frac{4R_v}{3.L_{total}(B_{mean} - 2e)}$$

5.3   Results

From Arch 1 to 10, the calculations described in Section 5.2 were performed for 18 sections. Table 9 lists all the sections considered, together with the factors against overturning and sliding (both considering and neglecting adhesion) and the base pressures if applicable.

When the soil friction angle, φ, is 30° and the wall friction angle, δ, is the half of φ, all sections have factors against sliding less than 1.0. Looking at the ratios for overturning, there is only one section that satisfies the criteria against overturning, namely Arch 6 with Buttress 6-5.

Table 9. Factor against overturning, sliding and base pressure states of all sections (φ=30°, δ=15°)

Section No.	Section	$F_{overturning}$	$F_{sliding}$		Base Pressure (MPa)	
			without adhesion	with adhesion	Maximum	Minimum
1	Arch 1 Buttress 1-2	0.651	0.281	0.388	Overturning	Overturning
2	Arch 2 Buttress 1-2	0.619	0.281	0.383	Overturning	Overturning
3	Arch 2 Buttress 2-3	0.583	0.263	0.355	Overturning	Overturning
4	Arch 3 Buttress 2-3	0.616	0.268	0.362	Overturning	Overturning
5	Arch 3 Buttress 3-4	0.530	0.239	0.321	Overturning	Overturning
6	Arch 4 Buttress 3-4	0.519	0.289	0.367	Overturning	Overturning
7	Arch 4 Buttress 4-5	0.449	0.214	0.285	Overturning	Overturning
8	Arch 5 Buttress 4-5	0.846	0.353	0.425	Overturning	Overturning
9	Arch 5 Buttress 5-6	0.976	0.383	0.462	Overturning	Overturning
10	Arch 6 Buttress 5-6	**1.036**	0.375	0.589	Not Applicable	Overturning
11	**Arch 6 Buttress 6-7**	**0.716**	**0.313**	**0.466**	Overturning	Overturning
12	Arch 7 Buttress 6-7	0.545	0.258	0.417	Overturning	Overturning
13	Arch 7 Buttress 7-8	0.438	0.252	0.401	Overturning	Overturning
14	Arch 8 Buttress 7-8	0.668	0.273	0.421	Overturning	Overturning
15	Arch 8 Buttress 8-9	0.653	0.278	0.424	Overturning	Overturning
16	Arch 9 Buttress 8-9	0.793	0.277	0.441	Overturning	Overturning
17	Arch 9 Buttress 9-10	0.793	0.333	0.500	Overturning	Overturning
18	**Arch 10 Buttress 9-10**	**0.843**	**0.347**	**0.511**	Overturning	Overturning

Since there was no available information about the buried parts of the Sections 1 to 6, the analysis was extensively dependent on the assumptions. Considering the uncertainties related to the cross sections, relatively lower ratios are admissible compared to those usually considered for new constructions.

The additional weight of the reinforced concrete balcony located on Buttress 5-6 and consequently wide accompanying Arches 5 and 6 lead to higher overturning and sliding stability of the section compared to the others. However, since the section is slightly above the overturning limit, the overturning and resisting moments are very close to each other. Consequently, the resultant vertical load which resists the net moment, is extremely close to the toe of the buttress base. The simplified method to compute the base pressures is not valid for this case, since a highly eccentric resultant force is positioned in front of the assumed average width, yielding a negative maximum pressure. Figure 58 shows that for Arch 6 with Buttress 5-6, the resultant force was located 6 cm away from the buttress toe while the edge of the average base width is 8 cm away from the same point. Therefore, the base pressures of the sections having factors against overturning that are very close to 1.0 cannot be estimated using this simplified approach.
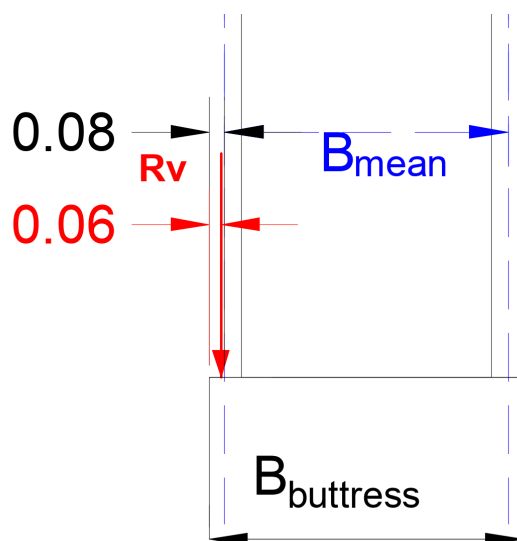
Figure 58. The position of the resultant vertical force of Section 6

5.4   Discussion of Results

The variations of the ratios throughout the wall are illustrated in Figure 59 and Figure 60. It can be stated that sliding is the critical failure mode over overturning for the entire wall. Both factors increase towards Section 10 as the weight of the unit increases and enhances the stability.

Sections 1 to 8, which were obtained from Arches 1 to 4 having similar characteristics in terms of inclination and the arches, are composing the part of the wall that was assumed to behave as a traditional gravity retaining wall with non-structural arches. From Section 1 to 8, the weight of the structure, the main stabilizing force, and the active pressure height increase simultaneously. As the increase in the overturning moments is more significant than the one in the stabilizing ones, the factor against overturning decreases. In the case of minor change in active pressure height, such as from Section 3 to 4, the increase in resisting moments governs, followed by an increase in the factor. From Figure 59, one can locate the sections from Arch 5 and 6 which have the highest factors due to additional weight of the reinforced concrete balcony and wider arches.
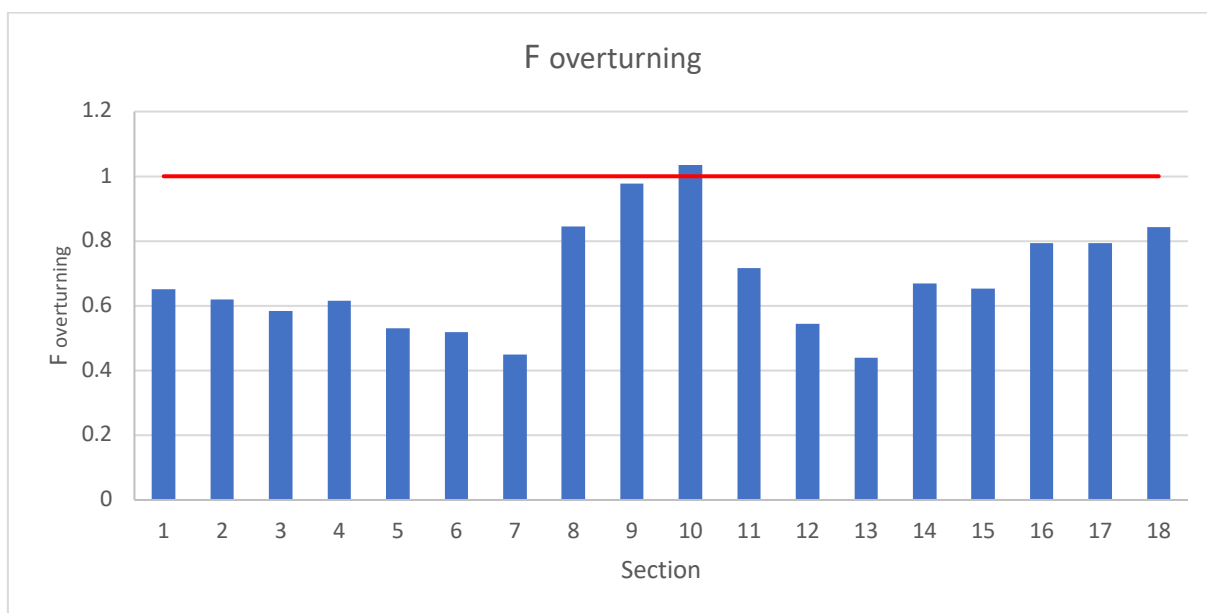
Figure 59. Factors against overturning

It is interesting to evaluate the effect of the wall inclination on overturning stability by comparing the parameters given in Table 10. Both of the stabilizing and overturning forces decrease from Section 15 to 16. The overturning moments decrease, on the contrary the stabilizing ones increase. The prominent difference between two sections that causes the phenomenon is the difference of buttress inclination. Since the moments were taken about the toe of the buttress, Section 16 making a lower angle with the horizontal causes the weights of the inclined members of the wall to have larger moment arms. Thus, despite the decrease in the magnitude of the resisting forces, resisting moments increase, enhancing the stability against overturning.

Table 10. Comparison of the overturning factors and their components of Section 15 and 16

Section	Arch 8 with Buttress 9-8	Arch 9 with Buttress 9-8
	15	16
R_v (kN)	1844.32	1607.64
P_a (kN)	1627.03	1428.01
$M_{resisting}$ (kN.m)	4028.89	4364.08
$M_{driving}$ (kN.m)	6165.66	5503.14
Buttress Inclination (°)	83	80
$F_{overturning}$	0.65	0.79

The soil layer at the foundation level was assumed to be changing from Layer A to B at Arch 6, which has a cohesion of three times the former one. The change of layer can be located from Figure 60 by the sharp increase at Section 10 (Arch 6 with Buttress 5-6) of the factor against sliding calculated by

considering the wall adhesion. Furthermore, the effect of wall adhesion on the factor against sliding is compatible at sections with constant cohesion value.
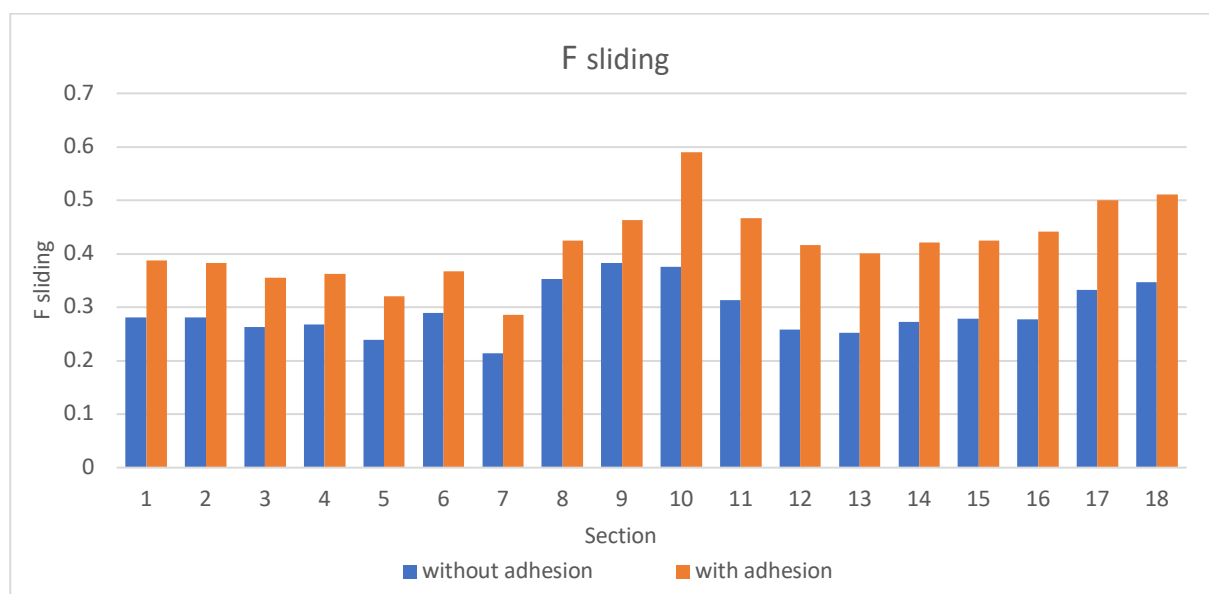

Figure 60. Factors against sliding

The fact that the shear strength parameters of the soil were obtained from a geotechnical survey that was performed 16 years ago and several meters away from the wall evokes uncertainties on the parameters. In addition, the soil friction angle and the undrained cohesion were correlated from SPT-N values of the layers, instead of laboratory testing such as Direct Shear or Triaxial Tests. This makes it very likely that they are overly conservative. Furthermore, foundation base being planar was a substantial assumption that alters the failure plane and the corresponding soil wedge that was considered during calculations.

Considering these factors, the ratios being smaller than 1.0 should not be interpreted as Mur Casa Salvans being unsafe as the wall has been stable for 100 years. In order to investigate the effect of the soil parameters on the stability factors, sensitivity analysis was performed on Sections 11 and 18, indicated with bold letters in Table 9. Arch 6 with Buttress 6-7 was selected as the representative unit of relatively small Arches 5-8 and Arch 10 with Buttress 9-10 as the representative unit of the larger ones. In addition, the computed factors against sliding and overturning of these sections were close to the average values of the groups they represent.

6   SENSITIVITY ANALYSIS ON SOIL SHEAR STRENGTH PARAMETERS

The sensitivity analysis was performed by modifying the soil and wall friction angles, φ and δ. Typical wall friction angle ranges depending on the backfill material are given in Table 11 [16]. The geotechnical report describes Layer A as sand slate and gravel with clay matrix. Owing to gravel content of the soil, the wall friction angle can be increased up to 30°. The stability analyses of all sections were performed for soil friction angles of 30°,35° and 40° and wall friction angles ranging from 1/2 φ to 30°.

Table 11. Wall friction angle ranges for different backfill materials

Backfill Material	δ (°)
Gravel	**27-30**
Coarse Sand	20-28
Fine Sand	15-25

Table 12 and Table 13 show the factors against overturning and sliding for different values of φ and δ for Arch 6 with Buttress 6-7 and Arch 10 with Buttress 9-10. The first rows of both of the tables list the values for the original case. It can clearly be seen that as φ and δ increase, both factors increase significantly. Both sections have factors larger than 1.0 from φ=35°and δ=27° onwards. It can be suggested that the actual values of the parameters might be larger or equal to these values.

Table 12. $F_{overturning}$ and $F_{sliding}$ of Arch 6 with Buttress 6-7 for different φ and δ values

φ (°)	δ (°)	$F_{overturning}$	$F_{sliding}$	
			Without adhesion	With adhesion
30	15.0	0.72	0.31	0.47
	17.5	0.75	0.38	0.54
	20.0	0.78	0.46	0.63
	27.0	0.87	0.70	0.91
	30.0	0.91	0.82	1.06
35	17.5	0.91	0.47	0.67
	20.0	0.94	0.56	0.77
	23.3	0.99	0.69	0.91
	27.0	1.04	0.84	1.10
	30.0	1.08	0.98	1.27
40	20.0	1.17	0.70	0.96
	23.3	1.22	0.85	1.14
	27.0	1.27	1.04	1.36
	30.0	1.31	1.22	1.57

Table 13. $F_{overturning}$ and $F_{sliding}$ of Arch 10 with Buttress 9-10 for different φ and δ values

φ (°)	δ (°)	$F_{overturning}$	$F_{sliding}$	
			Without adhesion	With adhesion
30	15.0	0.84	0.35	0.51
	17.5	0.89	0.42	0.59
	20.0	0.95	0.51	0.68
	27.0	1.09	0.78	0.98
	30.0	1.16	0.92	1.13
35	17.5	1.12	0.56	0.78
	20.0	1.17	0.67	0.89
	23.3	1.25	0.83	1.06
	27.0	1.33	1.03	1.27
	30.0	1.40	1.23	1.48
40	20.0	1.50	0.95	1.23
	23.3	1.58	1.19	1.48
	27.0	1.67	1.55	1.84
	30.0	1.75	2.01	2.26

In order to isolate the influence of φ it was assumed that δ was determined directly as 20° instead of correlating to φ. It can be seen from Figure 61 and Figure 62 that for both sections, the factors increase with φ following a similar trend, more drastically for $F_{sliding}$ of Arch 10 with Buttress 9-10 due to the larger weight and the base of this section.
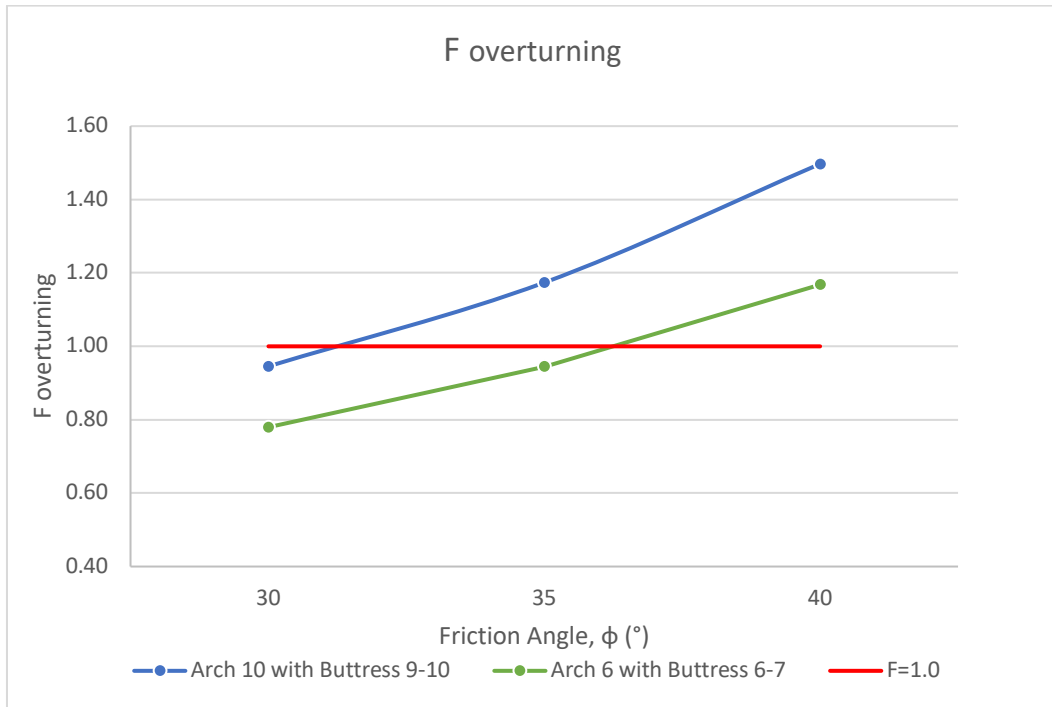
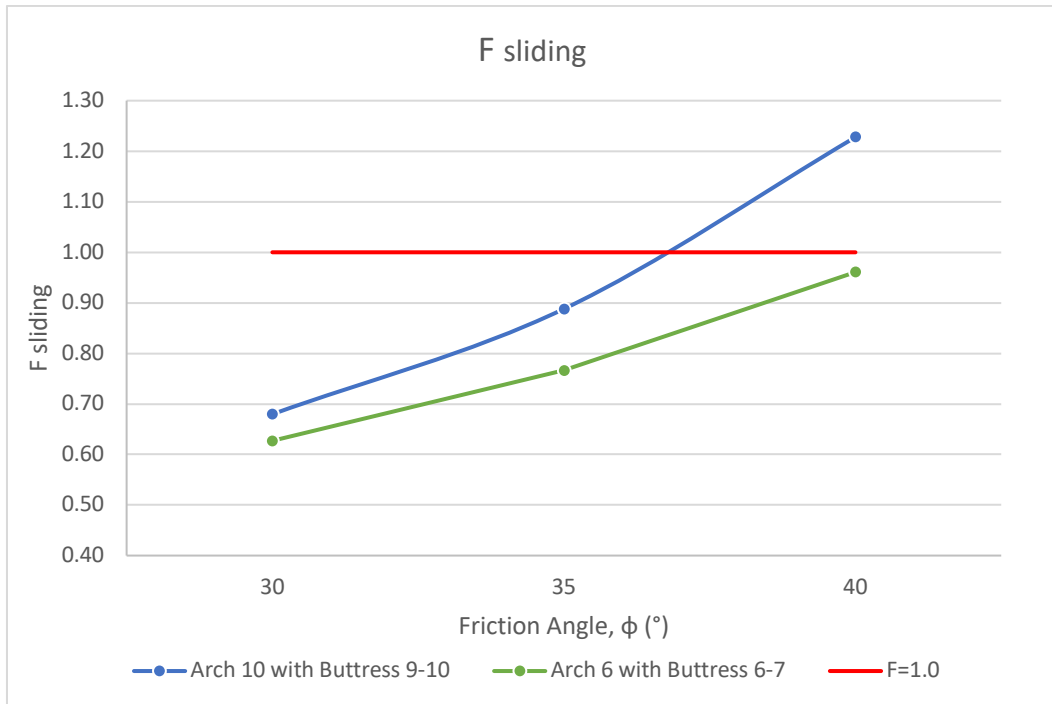Figure 61. Factor against overturning for different values of φ when δ=20°

Figure 62. Factor against sliding for different values of φ when δ=20°

Similarly, the effects of changing δ for different soil friction angles on both factors are illustrated in Figure 63 to Figure 66. For both sections, increasing δ alters the factor against overturning by a similar

trend regardless of the soil friction angle. However, the increase in the factor against sliding due to the increase of δ is higher as the friction angle gets higher and the section gets larger.
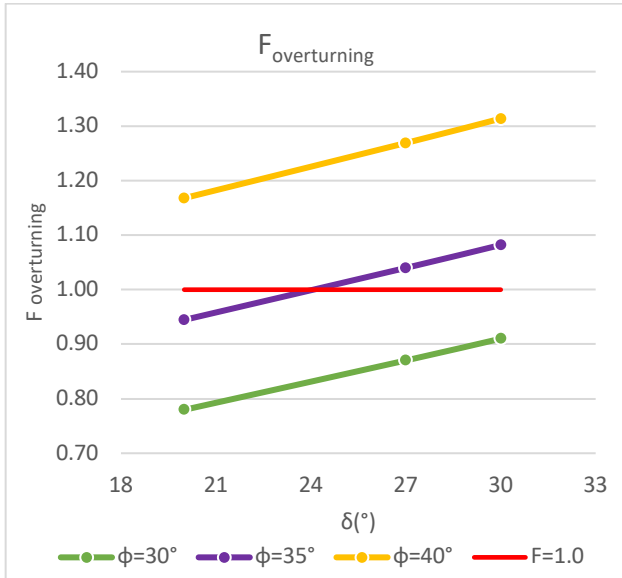

Figure 63. $F_{overturning}$ of Arch 6 with Buttress 6-7 for different values of φ and δ
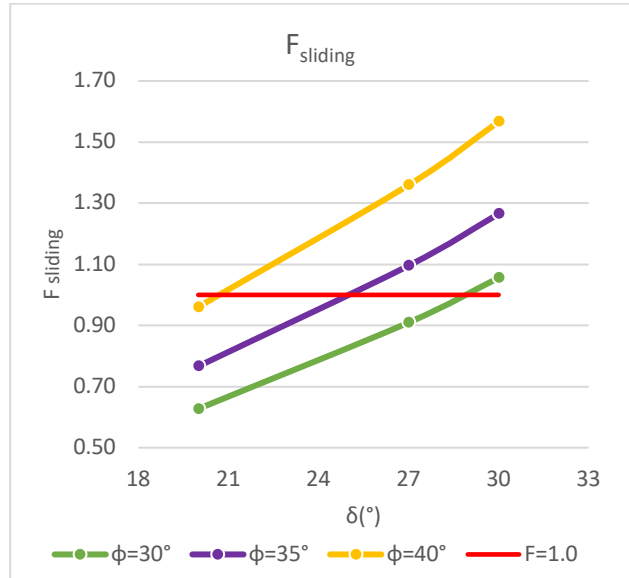

Figure 64. $F_{sliding}$ of Arch 6 with Buttress 6-7 for different values of φ and δ
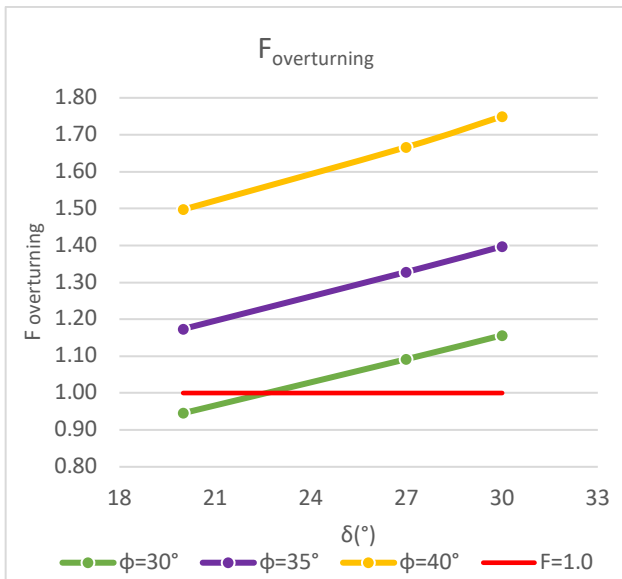

Figure 65. $F_{overturning}$ of Arch 10 with Buttress 9-10 for different values of φ and δ
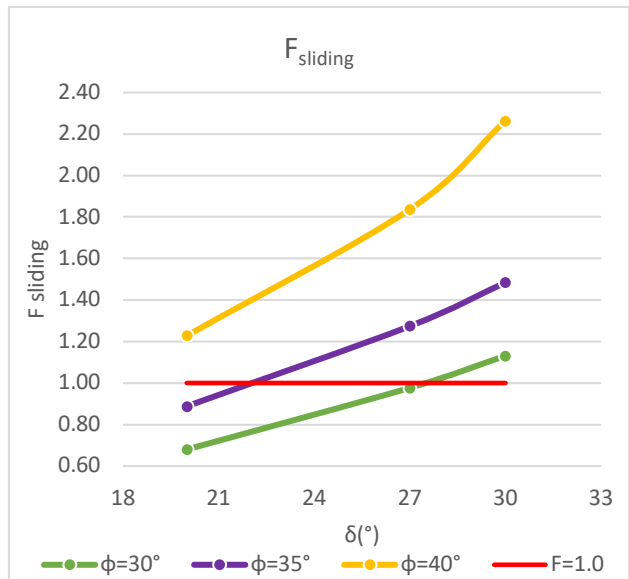

Figure 66. $F_{sliding}$ of Arch 10 with Buttress 9-10 for different values of φ and δ

Furthermore, since the overturning states of many sections vanish as the shear strength parameters of the soil increase, the base pressures may be investigated in greater detail compared to the initial case. Prior to the sensitivity analysis, Arch 6 with Buttress 5-6, Section 10 was the only section that was not overturning. Yet, the simplified method that was used to account for the varying base widths did not enable the base pressures to be computed. Table 14 shows all the sections for which the base pressures could be calculated for any case of sensitivity analysis. As discussed earlier in Section 5.3, when a section is just above the limit of overturning, its resultant vertical force is extremely eccentric and outside the assumed average base. As φ and δ increase, the resultants get more concentric, the simplified method can be applied and the estimated maximum base pressures decrease.

Table 14. Base pressure states of the computable sections for different values of φ and δ

		Maximum Base Pressure (MPa)										
φ (°)		**30**			**35**					**40**		
δ (°)		**15**	**17.5**	**20**	**17.5**	**20**	**23.33**	**27**	**30**	**20**	**23.33**	**27**
Section	8	O.Turning	O.Turning	O.Turning	N/A	4.42	1.71	1.07	0.84	0.58	0.51	0.45
	9	O.Turning	N/A	9.26	0.69	0.59	0.51	0.44	0.40	0.31	0.28	0.25
	10	N/A	3.61	1.63	0.49	0.45	0.40	0.36	0.33	0.23	0.20	0.20
	11	O.Turning	O.Turning	O.Turning	O.Turning	O.Turning	O.Turning	N/A	5.82	1.12	0.83	0.66
	14	O.Turning	O.Turning	O.Turning	O.Turning	O.Turning	O.Turning	O.Turning	N/A	19.97	1.91	1.01
	15	O.Turning	O.Turning	O.Turning	O.Turning	O.Turning	O.Turning	O.Turning	N/A	N/A	3.84	1.46
	16	O.Turning	O.Turning	O.Turning	N/A	N/A	3.15	1.10	0.76	0.41	0.36	0.32
	17	O.Turning	O.Turning	O.Turning	O.Turning	O.Turning	O.Turning	1.27	0.69	0.41	0.36	0.32
	18	O.Turning	O.Turning	O.Turning	O.Turning	O.Turning	O.Turning	1.15	0.67	0.46	0.36	0.25

In order to evaluate the effects of φ and δ on the maximum base pressure individually on Section 10, Arch 6 with Buttress 5-6, φ was modified when δ =20° and δ was modified when φ=35°. Figure 67 and Figure 68 show that despite the fact that an increase in each parameter decreases the base pressure, the effect of the soil friction angle is predominant.
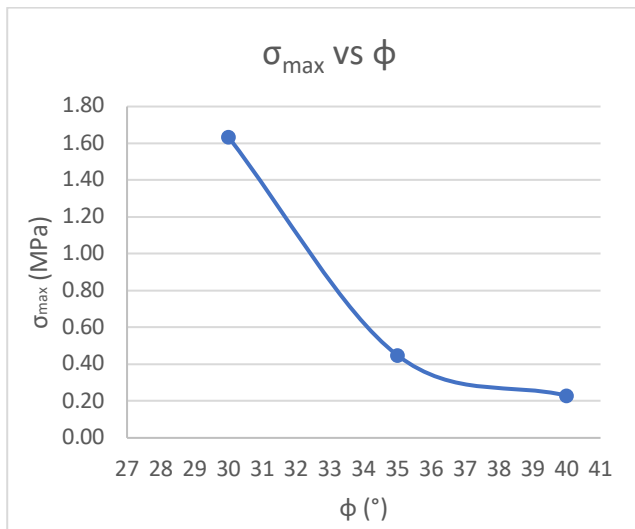
Figure 67. Maximum Base Pressure of Arch 6 with Buttress 5-6 vs φ when δ =20°
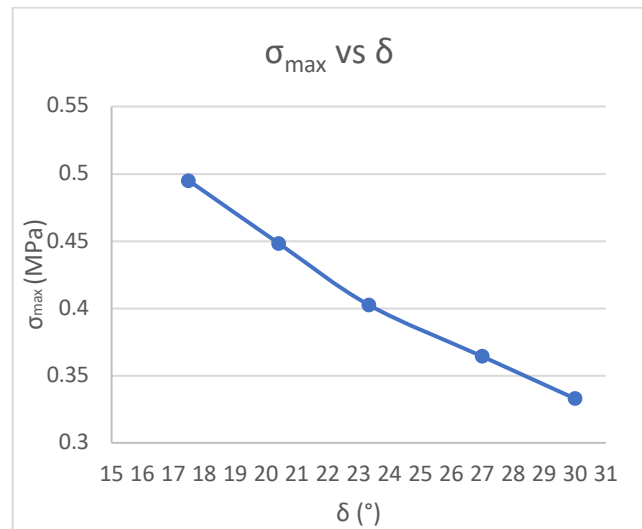
Figure 68.Maximum Base Pressure of Arch 6 with Buttress 5-6 vs δ when φ =35°

Changing the soil parameters enabled computing the base pressures, yet, it is not sufficient to comment on the possibility of failure due to base pressure. Again, the geotechnical survey derived the bearing capacities of the layers by correlations from SPT-N number. As the survey was performed in the area behind the wall, Layer B was classified as suitable for deep foundations due to its depth from the ground level. Tip resistance of the layer was given as 2.45 MPa [9]. Although it is not a compatible value to compare the base pressures due to its derivation, it can be seen that this value is exceeded by highly eccentric cases when $F_{overturning}$ is close to 1.0. Therefore, it would be erroneous to comment on the base pressures without further information about the foundation and soil characteristics.

7   GRAPHIC STATICS APPLICATION ON ARCH SERIES

7.1   Procedure

The thrust line is the load path along the arch, that is composed of the resultant compressive forces in equilibrium with the weight of the unit blocks of the arch, in an inverted catenary shape. Due to the thickness of the arch, there are infinite possible thrust lines within the arch, each of which are possible equilibrium solutions. Considering it is not possible to define the actual thrust line of any arch, the Lower Bound Theorem states that an arch can be deemed safe if a thrust line can be located within its boundaries. Therefore, in this chapter, fitting consequent thrust lines in the series of Arches 5-10 was aimed. For that purpose, graphic statics were applied on the arches starting from the left end of the wall, from Arch 10, proceeding towards the right by considering the dead load of the structure and the surcharge of 10 kN/m^2 on the soil above arch width.

The thrust lines were determined by means of a graphic statics tool that have inputs as the specific weights and dimensions of the arch, the buttresses and the filling. The tool considers that both of the buttresses and the arch are composed of 40 voussoirs that enables applying loads with respective eccentricities on individual voussoirs.

The procedure was demonstrated for Arch 10. Table 15 and Table 16 show the inputs that the tool requires. First, the origin was located at the left bottom corner of the buttress on the left side and required distances were obtained from AutoCAD. The measurement locations are illustrated in Figure 69.

Table 15. Buttress inputs of Static Graphics tool

	Buttress 1	Buttress 2
Upper width (m)	2.16	1.78
Lower width (m)	2.41	2.40
Thickness (m)	2.71	2.71
Height over reference (m)	10.39	9.97
Specific weight (kN/m^3)	22	22

Table 16. Arch Inputs of Static Graphics tool

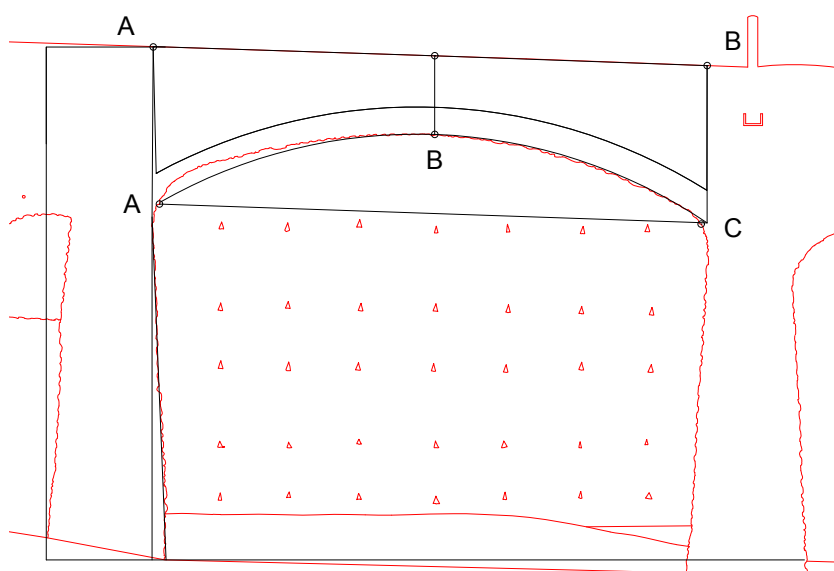|		
Arch	Span(m)	11.09
	Width(m)	2.10
	Height point A (m)	7.20
	Height point B (m)	8.61
	Height point C (m)	6.82
	Specific weight (kN/m^3)	22
	Thickness point A (m)	0.55
	Thickness point B (m)	0.55
	Thickness point C (m)	0.55
Filling	Height filling A (m)	10.39
	Height filling B (m)	10
	Specific weight (kN/m^3)	13.20

Figure 69. Locations of the measurements related to the arch and the filling

The tool was developed for rectangular buttresses. In order to reflect the inclination of the buttress edges towards the bottom, the voussoirs of the buttresses that are connected to the arch ends were determined from AutoCAD. The equations of the lines between those points to the corresponding ones at the bottom of the buttress were inserted in the cells defining the buttress boundaries. The left buttress of Arch 10 is connected to the half arch filled with masonry which provides additional buttress width at the lower part. After defining the arch, buttress and spandrel boundaries, the front view of Arch 10 with the buttresses was underlaid beneath the plot of the section geometry (Figure 70).
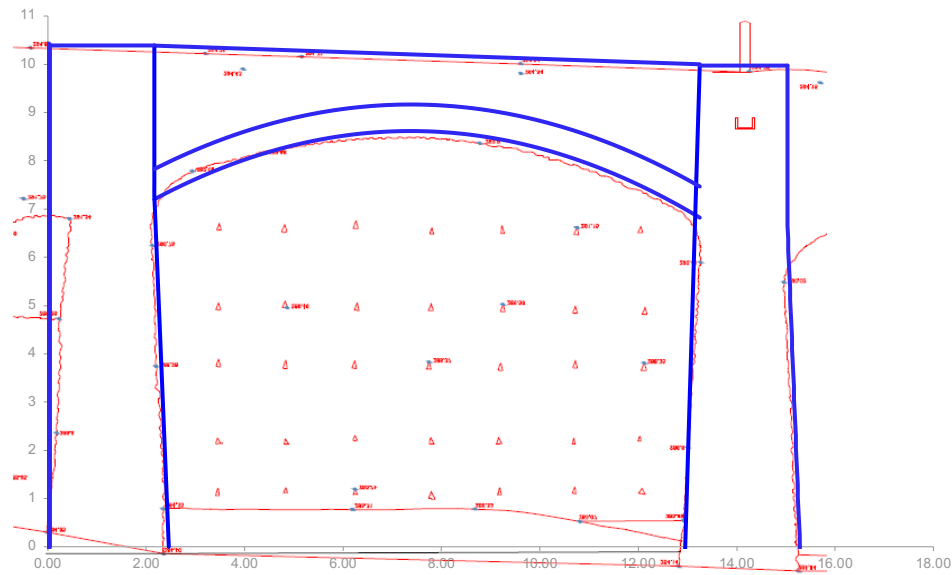
Figure 70. The chart defining Arch 10 with its buttresses

The wall was assumed to have spandrels of 40 cm thickness and soil until ground level above the arch. However, the tool considers the filling above the arch with the same thickness as the arch. In order to consider the vertical load above the arch accurately, the specific weight of the equivalent filling substituting the masonry spandrel and the soil was determined using the following procedure.

$$W_{soil\ above\ arch} + W_{masonry\ spandrel} = W_{infill}$$

$$\gamma_{fill} = \frac{A_{spandrel} \cdot t_{arch}}{W_{infill}}$$

Similarly, the buttress was considered to have a constant thickness over the height. The corresponding voussoirs having 40 cm thickness were determined and their thicknesses were changed accordingly.

The additional loads due to the soil mass above the buttresses, the extension on Buttress 9-10 and the reinforced concrete balcony on Buttress 5-6 were applied on the corresponding voussoir with their respective eccentricities. The surcharge acting on the soil surface was discretized to be applied on the arch voussoirs. The resultant of the surcharge was calculated by considering an area having the width of a voussoir and the thickness of the arch and applied on each voussoir as a point load. Finally, the voussoir of the right buttress having the thrust coming from the adjacent arch was determined.

Then a thrust line within the boundaries of the arch and the buttresses was determined by modifying four parameters in an iterative manner, namely the magnitude of the thrust, the eccentricities at the arch ends and the thrust applied by the following arch (Table 17). A similar procedure was followed for

the rest of the arches with an additional step of applying the thrust coming from the left arch at the corresponding voussoir. By modifying the same parameters, fitting a thrust line with the previously assumed magnitude of thrust was aimed. If it is not possible, the satisfactory thrust of the studied arch was transferred to the arch on the left at the corresponding voussoir. This procedure was repeated until a thrust is found that results in successive thrust lines in both of the arches.

Table 17. The tools used to fit the thrust line inside the arch

Thrust	kN	Eccentricities	m	m
◄ ►	500	◄► ◄►	-0.05	-0.30

7.2 Results

Figure 71 shows the thrust line of Arch 10 for a thrust of 670 kN when 660 kN thrust was assumed from Arch 9 at voussoir 16 of the right buttress. Considering the ability of the half masonry filled arch and the remaining wall on the left to resist thrust, the obtained thrust line is adequate.
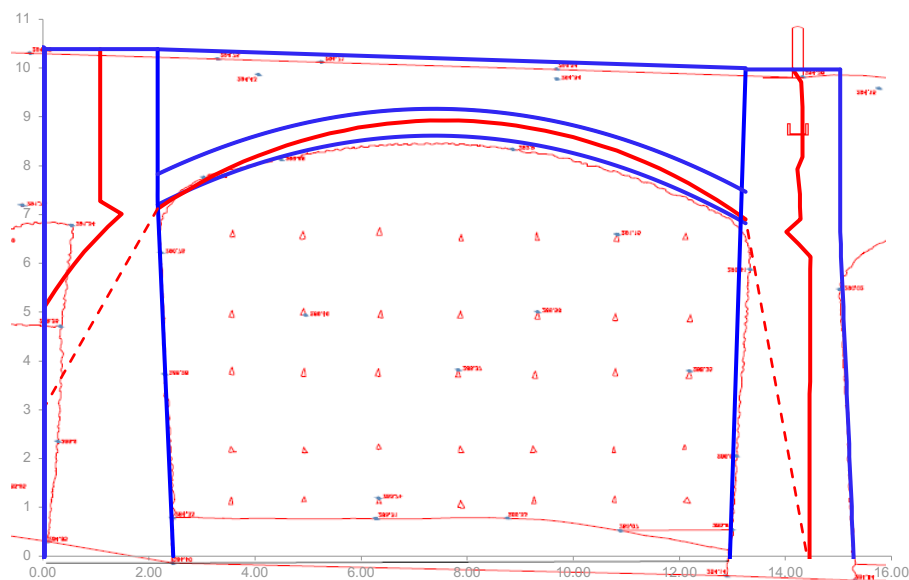

Figure 71. The thrust line of Arch 10 for F=670 kN

When Arch 10 applies 670 kN thrust on the left buttress and 630 kN from Arch 8 was assumed on the right one, a thrust line was obtained for the assumed 660 kN thrust for Arch 9 (Figure 72). Due to the large thrust applied by Arch 10, large eccentricity had to be assigned at the left end of Arch 9 to maintain the thrust within masonry. As a consequence, obtained thrust line is at the boundary of the

arch at extrados. However, the thrust line is acceptable as it lies within masonry boundaries and the actual arch thickness might be larger than 55 cm.
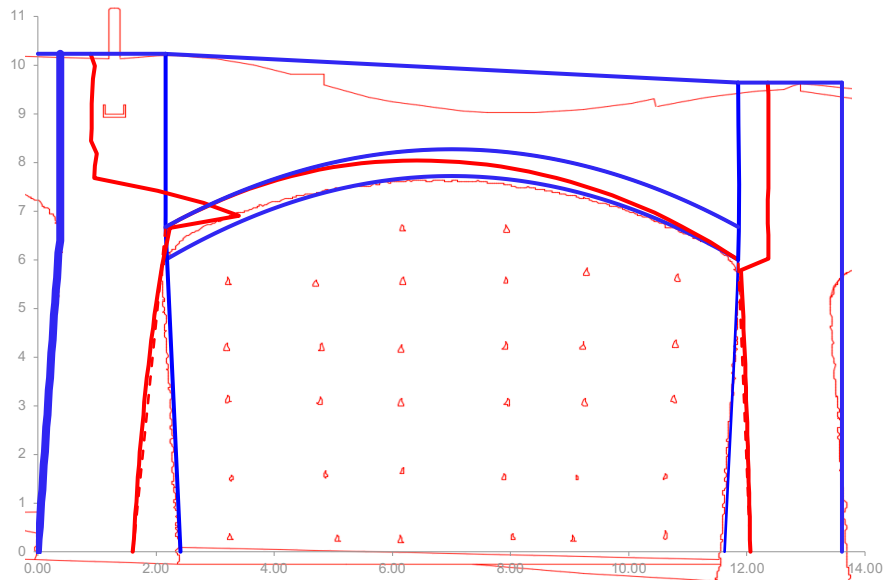

Figure 72. The thrust line of Arch 9 for F=660 kN

Subsequently, the thrusts of Arch 8 and 7 were determined as 630 kN and 550 kN, respectively. Obtaining smaller thrusts as the arch size decreases was anticipated (Figure 73 and Figure 74).The assumed thrust lines in the arch series imply the transmission of load from one arch to the next one through the buttresses, with contribution of the buttresses by taking some of the thrust.
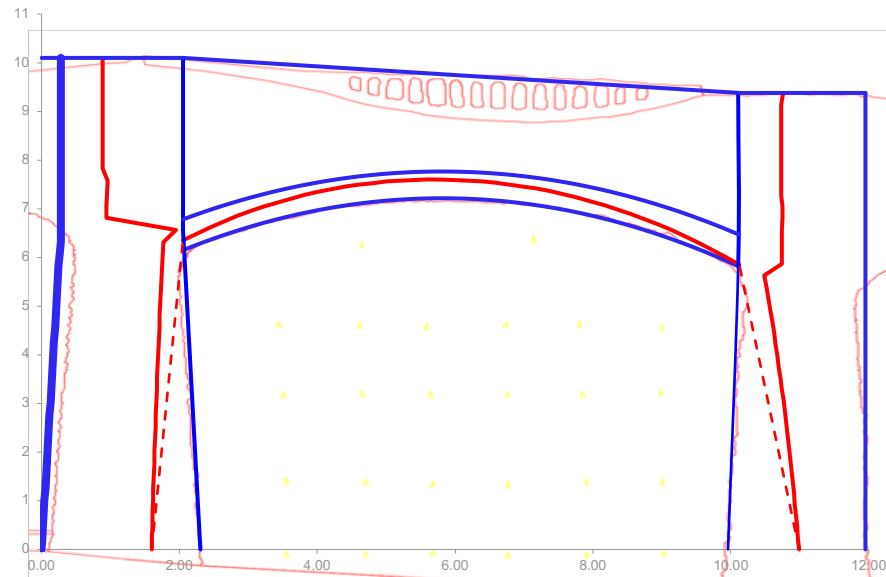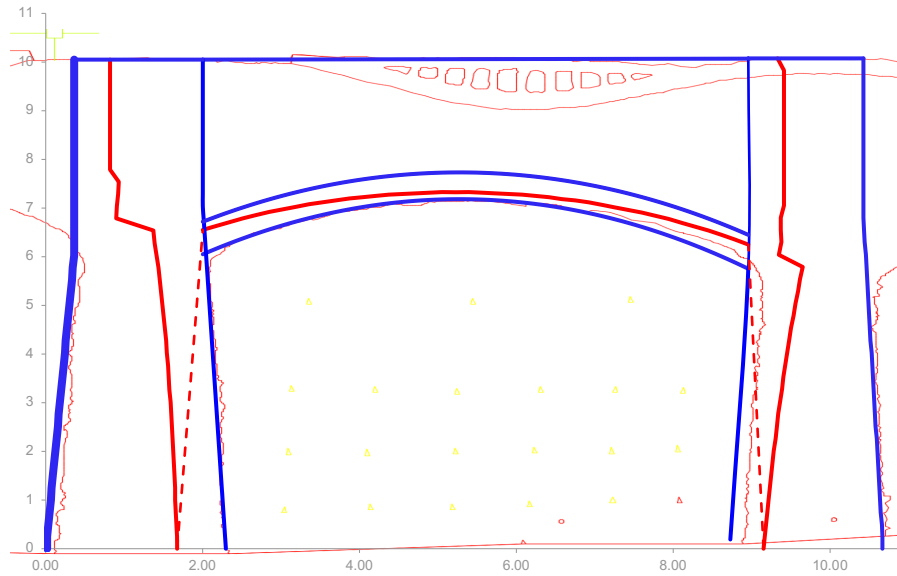

Figure 73. The thrust line of Arch 8 for F=630 kN

Figure 74. The thrust line of Arch 7 for F=550 kN

Due to the additional load of the cantilever balcony on Buttress 5-6, the descending trend of the thrust magnitude ends at Arch 6 (Figure 75). The last one of the series, Arch 5 shares the load of the balcony and has the large thrust from Arch 6 on the left buttress. In order to fit a thrust line within the arch, a 450 kN thrust from Arch 4 was assumed (Figure 76). Although Arch 4 was assumed to be a non-structural arch, considering the support it provides to Arch 5 as a wall is acceptable.
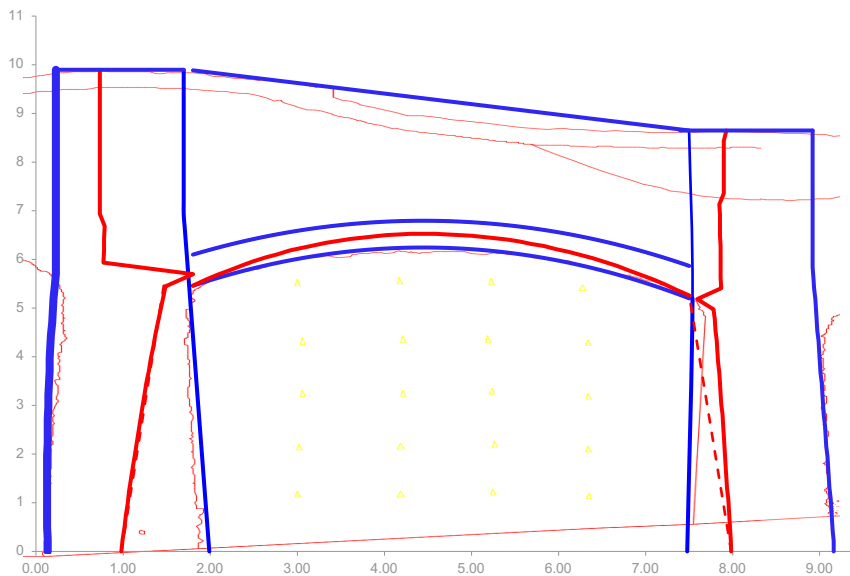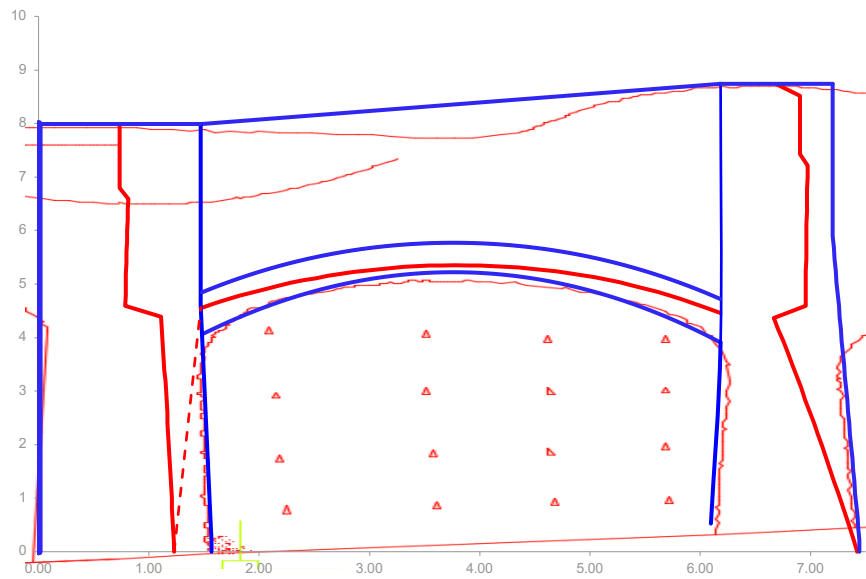

Figure 75.The thrust line of Arch 6 for F=600 kN

Figure 76. The thrust line of Arch 5 for F=570 kN

Figure 77 illustrates the magnitudes of the thrusts with descending arch number. The application of graphic statics on the arch series presumed the load transfer between the arches with some contribution of the buttresses by neglecting the wall below the arches. Since the thrust lines were situated within the arches in all cases, it can be concluded that the arch series is safe under given circumstances. No cracks being observed on site in any arch also validates the safety of the arches.
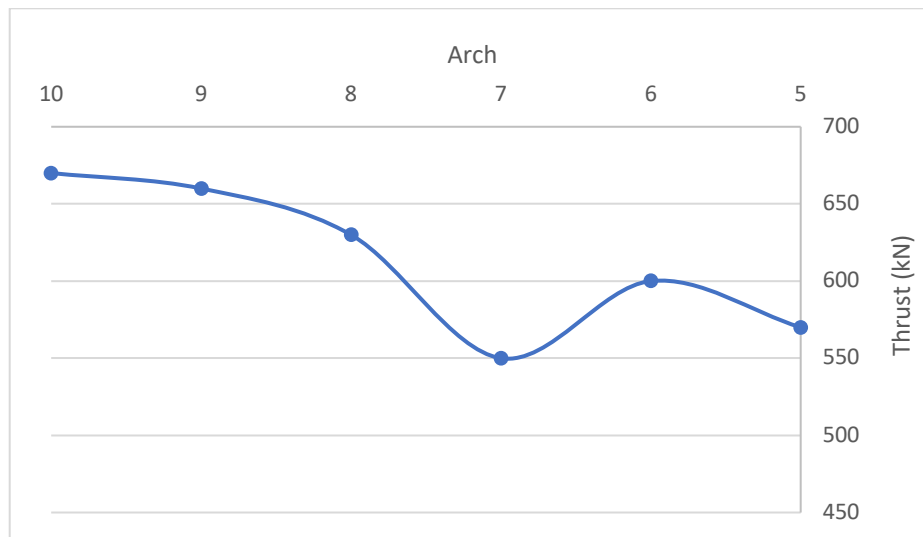

Figure 77. Thrusts vs Arches

This page is left blank on purpose.

8 CONCLUSION

In this study, it has been demonstrated that analysing the stability of an arched and buttressed retaining wall requires a detailed geometrical survey, which can be obtained by using a normal camera, and accompanying knowledge about the characteristics of the soil and the buried parts of the structure. Self-produced photogrammetric survey enabled capturing the geometry accurately, which defines the capacity of a retaining wall, of 10 arches located in Mur Casa Salvans. The three-dimensional photogrammetry models were combined with the available information from laser scanning, topographic and geotechnical surveys to construct the cross sections of the wall at different locations.

The main challenge of the assessment was to determine the representative unit sections to be analysed for stability. The geometry implies load transmission from the arches to the buttresses, indicating that the failure would be expected by the collapse of the buttresses in company with adjacent arches. Due to the unique geometry and alignment of each element, it was not possible to simplify the cross sections of the buttress and the neighbouring arches into a single one. Therefore, the wall was discretized into 18 units, between the buttress axis and the key of the following arch. The cross sections were created by making delicate assumptions on the hidden parts of the wall, to maintain a conservative approach. Due to the redundancy of the uncertainties, it was aimed to provide the least weight while maintaining the stability of the structure.

Then, a practical tool was developed to assess the stability of the unit sections in terms of overturning, sliding and base pressures. It can be used to analyze the stability of other retaining walls of given typology, if the necessary inputs are available namely, the densities of the material and the soil, shear strength parameters of the soil and the dimensions and inclination of the cross sections. Furthermore, the tool can be simply modified to consider the sections on both sides of the vertical axis of the buttress in cases of application on retaining walls having less complex, more uniform geometry.

As a consequence of aforementioned conservative assumptions, the wall did not comply with modern retaining wall design standards, which was quite anticipated. It should be noted that these factors should not be interpreted as safety indicators for existing soil retaining structures. The more uncertainties involved, the lower were the factors against overturning and sliding, such as the factors for the smaller arches where there was no available information about the buried parts of the structure. As the weight of the section increases, both factors against overturning and sliding increases. In addition, the factor against sliding also increases when the section has a wider foundation base.

With the assumed soil shear strength parameters of φ =30° and δ=15°, only one section, Arch 6 with Buttress 5-6 where the reinforced concrete balcony is located together with the widest arch of the wall,

has a factor against overturning larger than 1.0. However, Mur Casa Salvans can be deemed as stable in terms of overturning, considering the calculations were carried out for the least possible weight. Assumptions of parallel back face of the wall to the front, 60 cm buried thickness both for the buttresses and the wall and no masonry mass above arch level can easily be quite different in reality. It has also been found out that a slight decrease in inclination, measured from the horizontal, improves the overturning stability significantly, due to the increase in lever arms of the weight components. It has been demonstrated that the wall is more vulnerable to sliding than to overturning. Not only the uncertainties on the actual foundations, but also the soil parameters being correlated from SPT-N values can be suggested as the grounds of the phenomenon. The geotechnical survey not being up to date and providing information from boreholes relatively far away from the wall raises doubts on the reliability of those parameters.

Thereby, a sensitivity analysis was carried out which enabled to observe the evolution of the factors with slight changes of φ and δ, individually. The results of the investigated sections imply that when φ =35° and δ=27° or larger, the factors are greater than 1.0. These values may be suggested as the possible minimum values of the real parameters, if the wall was to have the assumed geometry. Although increasing φ increases both of the factors, the increase in factor against sliding is more significant in the larger sections, due to wider base areas. Similarly, δ improves the factor against sliding more than the overturning one, due to the increase of the adhesion at the base.

In order to determine the base pressures, further information is required related to the characteristics of the foundation and the actual heights of active and passive pressures. In the thesis, a simplified approach was used to estimate base pressures while considering the varying base widths within a unit section. Sensitivity analysis reveals that after a section surpasses the overturning limit, the base pressures decrease, while the resultant vertical load gets more concentric, as φ or δ increases. The effect of soil friction angle is predominant on the base pressures.

Finally, the stability of the arch series has been verified by sequential application of static graphics on the arches. From infinite possible thrust lines, a thrust line has been successively established for each arch while considering the thrusts of the adjacent ones. The magnitudes of the thrusts comply with the configuration of the wall, as decreasing with the decrease in the arch size, but increasing towards the additional load of reinforced concrete balcony at one of the buttresses. The identified thrusts indicate that, if the arches were having the determined thrust lines in reality, all the load above arch level would be transmitted from one arch to the other, by some contribution of the buttresses.

Future works to assess the stability of Mur Casa Salvans require further inspection of the wall. Morphology and thickness of the wall can be determined by minor destructive methods such as Boroscopy which provides visual access to inaccessible parts of the structures. Considering the

geometrical variations throughout the wall, by means of drilling sufficient number of holes, the characteristics of the hidden parts of the wall can be determined. Furthermore, performing a more comprehensive geotechnical survey is essential to assess the stability of the wall accurately. In order to determine the present soil layers at different levels of the wall, boreholes should be located closer to the wall compared to the previous survey. In addition, undisturbed soil samples should be taken to be tested in the laboratory. Considering the non-cohesive characteristics of the layers, shear strength parameters should be determined by means of Direct Shear Test. In order to determine the bearing capacity of the layers, Standard Penetration Test could be performed. Finally, if possible, with the required permissions about the damage that will be caused in the adjacent road, wider and deeper excavations should be performed at the base of the wall to reveal the morphology of the foundation.

9   REFERENCES

[1]   M. Xiao, *Geotechnical Engineering Design*, First Edit. West Sussex: WILEY Blackwell, 2015.

[2]   M. Fontanese, "A Stability Analysis of The Retaining Walls of Machu Picchu," University of Pittsburg, 2010.

[3]   H. Brooks and J. P. Nielsen, *Basics of Retaining Wall Design*, 10th Editi. Newport Beach: HBA Publications, 2013.

[4]   R. F. Craig, *Craig's Soil Mechanics*, 7th Editio. London: Spon Pres, 2004.

[5]   S. Huerta, "Mechanics of masonry vaults: the equilibrium approach," *Proc. 1st Int. Congr. Struct. Anal. Hist. Constr. Guimaraes*, pp. 47–70, 2001.

[6]   P. Roca and P. Lourenço, "Ancient Rules and Classical Approaches Part 1."

[7]   S. I. Granshaw, *Close Range Photogrammetry: Principles, Methods And Applications*, vol. 25, no. 130. 2010.

[8]   T. Municipality, "Cataleg D'edificis D'interés Historic Artistic Del Terme Municipal de Terrassa."

[9]   GESOND S.A., "Estudi Geotecnic No: 18877 d'un Sector Situat Entre el Carrer Salmeron S/N, El Parc de Vallparadis i El Museu de Textil de Terrassa," 2003.

[10]   iHandy, "iHandy Carpenter." 2017.

[11]   Autodesk, "ReCap Photo." Autodesk, 2019.

[12]   CloudCompare, "CloudCompare Version 2.10.alpha [GPL Software]." 2018.

[13]   Autodesk, "AutoCAD." 2019.

[14]   NTC 2008, "CIRCOLARE 617.2009 - Istruzioni per l'applicazione delle NTC 2008 (appendice)," pp. 355–434, 2009.

[15]   B. S. I. BSI, "EC1: Part 1.1: Densities, self-weight, imposed loads for buildings," *Structural Engineer*, vol. 82, no. 2. European Comittee For Standardization, London, p. 44, 2002.

[16]   B. Teymur, "Earth Pressures and Retaining Walls," İstanbul.

10 ANNEX

1.1 Topographic Survey of Mur Casa Salvans

Pit 1

- Location: Base of the wall at Section 1
- Pipelines were found at 40 cm depth of excavation.

Figure A.1.Pipelines in Pit 1

Pit 2

- Location: Top of the wall at Section 1
- Depth of excavation: 120 cm
- Balustrade height: 100 cm
- Balustrade width: 30 cm
- Width of the wall: 65 cm

Pit 3

- Location: Base of the wall on the left side of Buttress 2-3
- Depth of excavation: 75 cm

Figure A.2.Pit 3 below Arch 3, on the left side of Buttress 2-3

Pit 4

- Location: Top of the wall, on the key of Arch 3
- Change of wall width from 40 cm to 60 cm observed at a depth of 155 cm measured from the top of the balustrade.

Pit 5

- Location: Top of the wall, on Buttress 2-3
- Depth of excavation: 135 cm without locating the arch.

Pit 6

- Location: Top of the wall, on Buttress 5-6
- Concrete block of 150 cm height detected at 30 cm depth, measured from the ground level.

Figure A. 3(a) A Balcony section located on Buttress 5-6 from top. (b) Pit 6 on Buttress 5-6
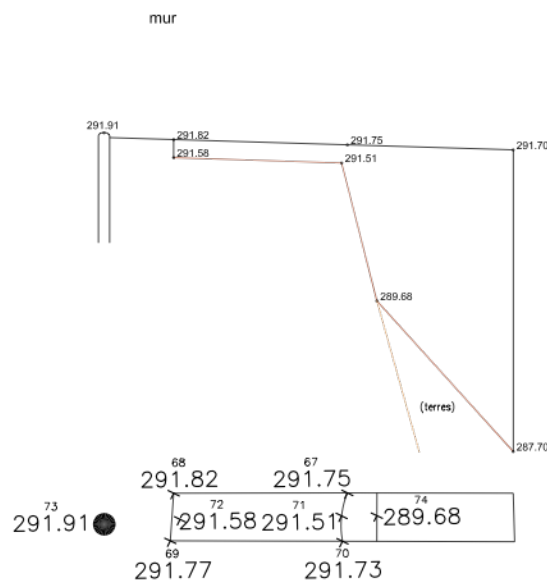
Figure A. 4. Cross Section of Pit 6

Pit 7

- Location: Base of the wall, on the left side of Buttress 5-6

Figure A. 5. (a) Pit 7 on the left side of Buttress 5-6 (b) Location of Pit 7

Pit 8

- Location: Top of the wall, on the key of Arch 6
- Balustrade width: 40 cm
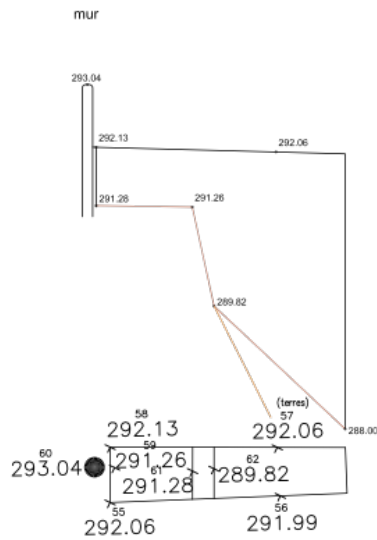

Figure A. 6. Cross section of Pit 8

Figure A. 7. Pit 8 on the key of Arch 6 from different angles

Pit 10

- Location: Top of the wall, on Buttress 6-7

- Balustrade height: 90 cm

- Concrete block of 60 cm height detected at 90 cm depth measured from ground level.

Figure A. 8. (a) Pit 10 on Buttress 6-7 (b) Cross Section of Pit 10

Pit 11
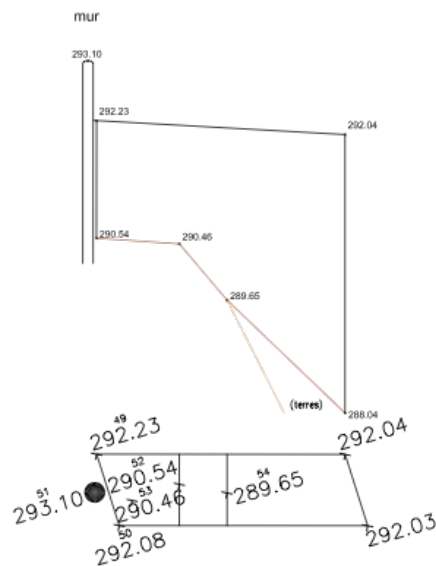
- Location: Top of the wall, on the key of Arch 7

Figure A. 9. Pit 11 on the key of Arch 7 (b) Cross section of Pit 11

Pit 12

- Location: Base of the wall on the left side of Buttress 7-8

- Depth of excavation: 80 cm

- Concrete base detected.
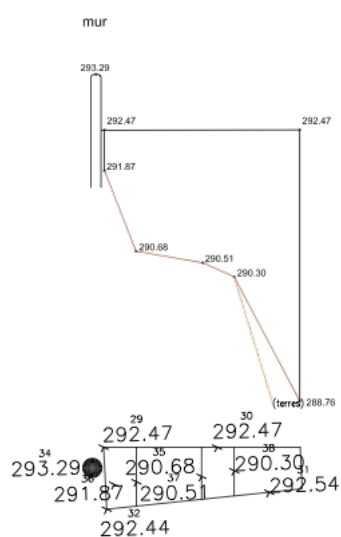

Figure A. 10. Concrete base found in Pit 12

Figure A. 11. Location of Pit 12 (b) Cross Section of Pit 12

Pit 13

- Location: Top of the wall, on the Buttress 7-8

Figure A. 12.Pit 13 on top of Buttress 7-8

Pit 14

- Location: Top of the wall, on the key of Arch 8
- Balustrade height: 90 cm

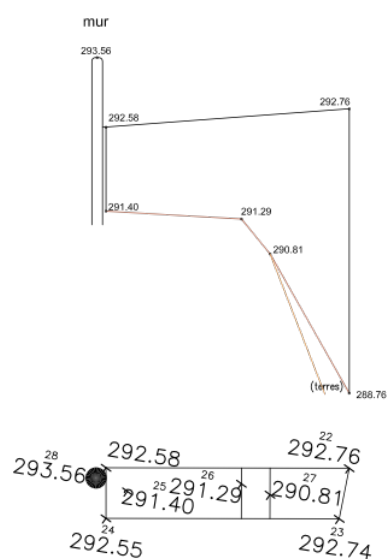

Figure A. 13. Pit 14 on the key of Arch 8

Figure A. 14. Cross Section of Pit 14

Pit 15

- Location: Base of the wall, on the Buttress 8-9
- Concrete base detected.
- Concrete base width: 35 cm
- Concrete base depth: 115 cm

Figure A. 15. Concrete base found in Pit 15

Pit 16

- Location: Top of the wall, on the Buttress 8-9
- Balustrade height: 90 cm
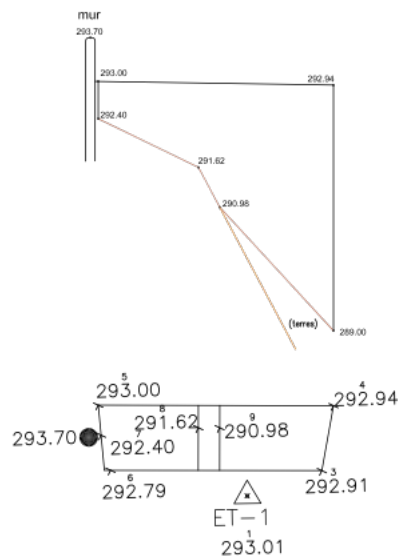

Figure A. 16.Pit 16 on top of Buttress 8-9

Figure A. 17. Cross Section of Pit 16

Pit 17

- Location: Top of the wall, on the key of Arch 9

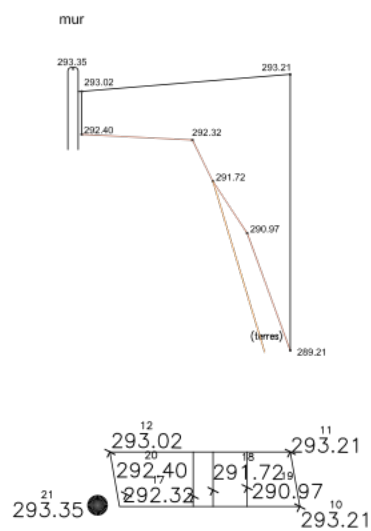Figure A. 18. Pit 17 on the key of Arch 9 from different angles

Figure A. 19. Cross section of Pit 17

Pit 18

- Location: Base of the wall, on the left side of the Buttress 9-10
- Concrete base detected.
- Concrete base width: 20 cm
- Concrete base depth: 230 cm
- After the excavation of 230 cm, a rebar was driven into the ground for 50 cm. Yet, the foundation was not detected.

Figure A. 20. Pit 18 on Buttress 9-10

Pit 19

- Location: Top of the wall, on the Buttress 9-10
- Next to the boundary of a private property.

Figure A. 21.Pit 19 on the top of Buttress 9-10

Pit 21

- Location: Base of the wall, on the right side of Buttress 10-11
- Concrete base detected at 50 cm depth measured from the ground level.
- Concrete base width: 40 cm

Figure A. 22. Pit 21 on Buttress 10-11